7-2-2012

Simulation of optical impacts of gravity-induced deformations of concentrating solar collectors

Joshua Christian

Joshua Christian

Candidate

Mechanical Engineering

Department

This thesis is approved, and it is acceptable in quality and form for publication:

Approved by the Thesis Committee:

Dr. Andrea Mammoli , Chairperson

Dr. Chris Hall

Dr. Clifford Ho

Simulation of Optical Impacts of Gravity-Induced Deformations of Concentrating Solar Collectors

By

Joshua Christian

Previous Degrees
Bachelors of Science in Mechanical Engineering

THESIS

Submitted in Partial Fulfillment of the
Requirements for the Degree of

Master of Science

Mechanical Engineering

The University of New Mexico
Albuquerque, New Mexico

May, 2012

ACKNOWLEDGMENTS

I would like to acknowledge my mentor, Dr. Clifford Ho, who has given me excellent insight, advice, and introduced me to the wide world of system modeling for solar energy research. He has given me valuable experience and has inspired me to continue working in the solar energy sector.

I also wish to thank Tim Moss, Rich Diver, and Gregory Kolb for their insightful discussions and assistance with the LS-2 trough modeling. Their help has been priceless during this research.

I would like to thank Dr. Andrea Mammoli for being a great advisor. He has provided me a stable direction for this ongoing research opportunity.

I would like to thank all of my committee members including Clifford Ho, Andrea Mammoli, and Chris Hall. They have given up valuable time to help me fulfill my Master's degree and I am truly grateful.

I would like to thank my loving wife for her patience and support through the long hours of work and writing to accomplish this research.

Simulation of Optical Impacts of Gravity-Induced Deformations of Concentrating Solar Collectors

by

Joshua Christian

B.S., Mechanical Engineering, New Mexico Institute of Mining and Technology, 2010

ABSTRACT

Concentrating solar power (CSP) is a large field of interest in the renewable energy sector. However, CSP has not yet become as economical as other renewable energy technologies. A possible solution to this issue is the ability to produce efficient and cost-effective solar collectors such as parabolic troughs, heliostats, and parabolic dishes. There are many different areas where costs can be reduced such as using cheaper materials, developing more efficient power cycles, designing better structures, reducing the control system cost, or improving the alignment of the mirrors. The research presented focuses on the area of mirror alignment. Properly aligned mirrors produce more concentrated solar energy output thereby increasing the thermal efficiency in the entire system.

The first purpose of this research is to develop a cost-effective method to analyze gravity deformations in solar collectors. The deformations are found from Finite Element Analysis (FEA) on a true scale model. The second purpose of this research is to study the optical performance of the solar collector after gravity deformation. Ray tracing is used to fully analyze the optical performance of collectors. Together the deformations and beam characterization lead to a useful, cost-effective process to analyze solar collectors.

The results of the study show that the simulations presented can accurately match experimental data. The final process allows for design changes to be studied before making a costly prototype.

Table of Contents

LIST OF FIGURES

x

LIST OF TABLES

DEFINITIONS

FEA is the standard acronym for Finite Element Analysis.

An FEA **element** refers to the discrete piece of an FEA model. Each element contains **nodes** which are used to solve the stress and strain equations at those specific points.

A **displacement** is defined as the translation and rotation of an FEA element from its original location after loading. This is reported in three dimensions using a standard length unit such as millimeter or inch. The term deformation is also used to describe displacements.

A **surface normal** is the vector normal to a particular surface.

A **slope error** is defined as the angular deviation of the surface normal vector of a finite element before and after loading. The surface normal of a finite element is known before loading and the new surface normal of that same element can be determined after loading. A slope error is commonly used to describe the optical accuracy of a reflecting surface. A perfectly reflecting surface wouldn't have any slope errors. Slope errors occur from loadings, but there are inherent mirror inaccuracies induced during manufacturing and assembly processes.

An **HCE** is the standard abbreviation for the heat collecting element of a parabolic trough. It is usually composed of an external glass envelope which surrounds a heat absorbing element.

A **ray trace** is a simulation which tracks photons (rays) from an emitting source. The rays are allowed to be reflected, absorbed, or transmitted by objects in the ray trace model.

For a parabolic trough the **intercept factor** is the main optical performance metric. An intercept factor is the ratio of actually energy on the heat collecting absorbing element to the total energy reflecting from the collector surface. A perfectly reflecting solar collector without deformations will result in an intercept factor of 1 since all of the energy reflecting from the collector surface will impact the HCE absorbing element. Other collector systems such as heliostats rely on flux maps and beam shape to quantify optical performance. These metrics are easily found using plane targets during ray tracing.

An **incident angle** is the angle between the normal of the collecting surface to the aperture and the incoming solar rays. This angle is used to evaluate solar collector performance when tracking the sun throughout the day. It is expected that a larger incident angle results in more energy missing the HCE resulting in a lower intercept factor.

An **incident angle modifier** accounts for deviations from a zero incident angle between the sun and the collector for experimental studies. It is defined as the efficiency of the trough at any incident angle to the sun divided by the efficiency of a trough at zero incident angle to the sun.

When a ray trace emitting source is set to emit photons (a ray), the ray is emitted within a defined solid angle (cone angle). An **apodized** source means that the intensity of the energy leaving the source in a ray is non-uniform along the defined emitting cone angle.

1. INTRODUCTION

Concentrating solar power (CSP) is a large field of interest in the renewable energy sector. However, CSP has not yet become as economical as other renewable energy technologies. A possible solution to this issue is the ability to produce efficient and cost-effective solar collectors such as parabolic troughs, heliostats, and parabolic dishes. There are many different areas where costs can be reduced such as using cheaper materials, developing more efficient power cycles, designing better structures, reducing the control system cost, or improving the alignment of the mirrors. The research presented here focuses on the area of mirror alignment. Properly aligned mirrors produce more concentrated solar energy output thereby increasing the thermal efficiency in the entire system.

Understanding the impacts of gravity loading on collectors can improve mirror aligning procedures. Using the known gravity deformations in alignment procedures is known as biasing. Biasing can lead to more accurate mirror alignment possibly resulting in more power output of solar collectors. The first goal of this research is to develop a cost-effective method to analyze gravity deformations in solar collectors. The deformations are found from Finite Element Analysis (FEA) on a true scale model. The second goal of this research is to study the optical performance of the solar collector after gravity deformation. Ray tracing is used to fully analyze the optical performance of collectors. Together the deformations and beam characterization lead to a useful, cost-effective process to analyze solar collectors. The process allows for design changes to be studied before making a costly prototype. Usually, a prototype is built and then optical

analysis is performed through experiments. In this study an LS-2 parabolic trough will be analyzed as an example for the procedure developed in this study.

2.   BACKGROUND

Solar Collectors range in size and shape in order to concentrate sunlight onto a particular target. Typical collectors are heliostats, parabolic troughs, and parabolic dishes. The procedure being developed can be used for any of the geometries, but as an example a parabolic trough will be studied. The LS-2 parabolic trough was designed and developed by LUZ Industries and is used at the Kramer Junction Solar Electric Generating System (SEGS) in Southern California. This particular trough has a mirror aperture of 5 m and a focal length of 1.49 m. A complete LS-2 parabolic trough consists of six trough modules with each module containing five columns of four mirrors. The total length of a complete trough system is 49 m long [1].

When considering the optics of a solar collector the focal length is often referenced. In a parabolic trough, the rays are all focused to a single focal length along the length of the trough. This line is called the focal line. A plane of curvature is also described and this is a cross-sectional plane of the parabolic trough. Figure 1 represents the basic geometry of the parabolic trough collector. A parabolic trough is a line-focus collector which means all of the solar energy is reflected to the focal line along the axis of the parabolic trough. The only requirement for the incoming solar energy is that rays are parallel to the 'normal to aperture' of the collector when projected onto the plane of curvature. This results in the solar energy being reflected to the focal line with accuracy. Figure 2 depicts the tracking required by the trough at different sun positions. To achieve this, a parabolic trough requires one axis of rotation to track the sun throughout the day.

A torque tube is responsible for mirror rotation and rotates the entire trough collector in the same way to track the sun. A typical parabolic trough solar plant aligns the parabolic troughs in an East to West axis orientation or a North to South axis orientation depending on the location of the plant.
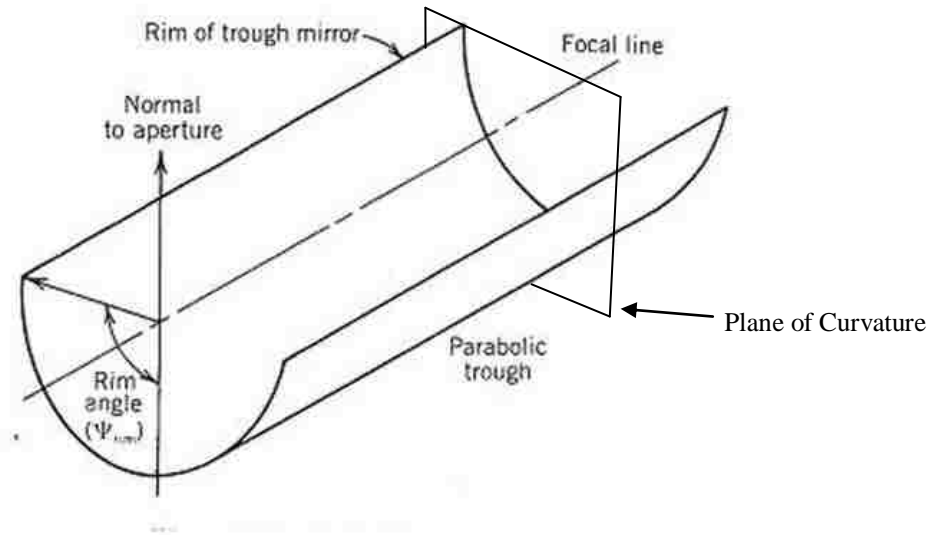
Figure 1. Simple parabolic trough geometry diagram [2]
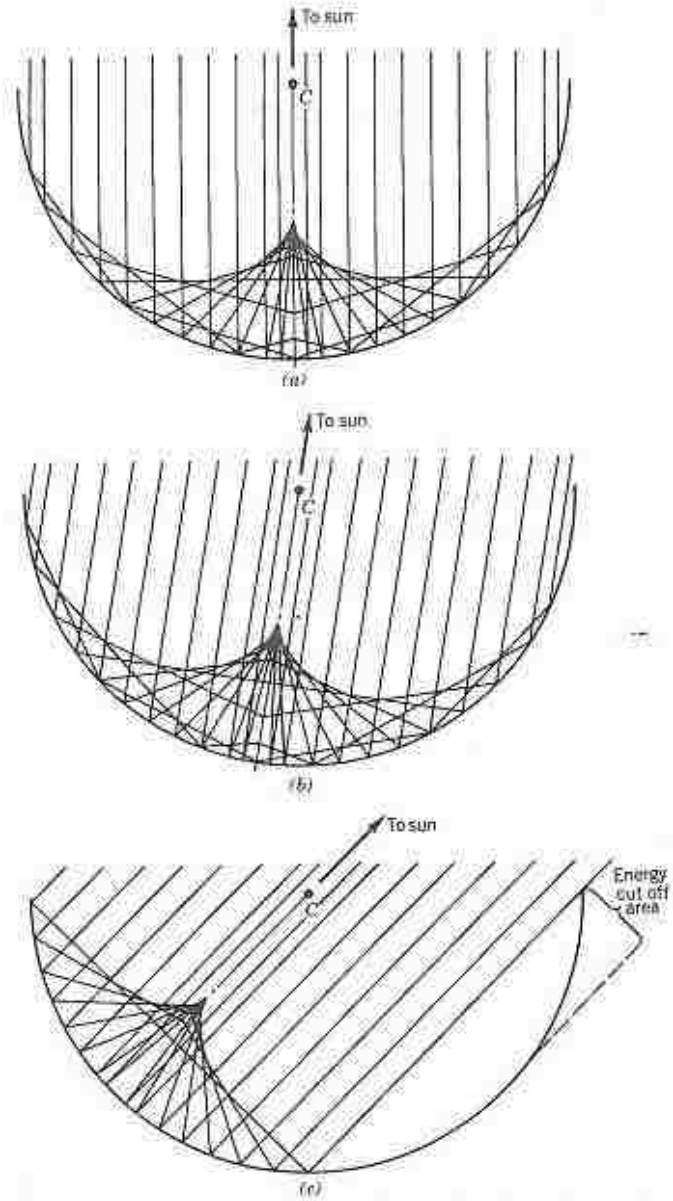
Figure 2. Parabolic trough with solar energy rays parallel to the normal to aperture of trough and reflecting to the focal line at different trough rotations to account for differing sun positions [2]

A parabolic trough power plant combines many parabolic solar collectors in order to drive the electrical generation process. The basic elements of a collector are the torque tube, mirrors, and heat collecting element (HCE). The torque tube rotates the trough so that it properly tracks the sun throughout the day. The mirrors reflect the solar energy

from the collector to the focal line of the trough. The HCE is placed at the focal line of the trough and is responsible for absorbing the solar energy reflected from the collector. A heat transfer fluid (HTF) is pumped through the HCE and absorbs the solar energy incident on the HCE. Figure 3 depicts how the parabolic troughs would be combined in an actual power plant to produce thermal energy for electricity production. The trough rotates about the axis of the trough which runs along the length of the torque tube.
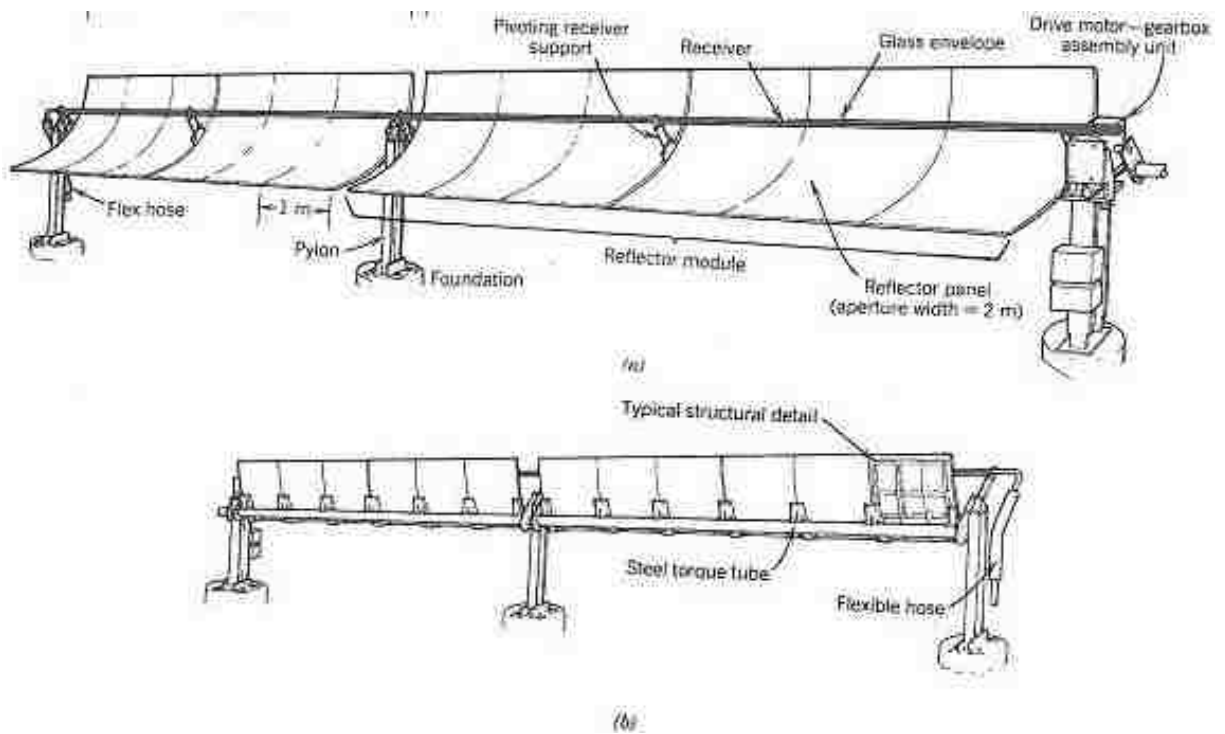
Figure 3. Typical parabolic trough power plant setup [2]

A single LS-2 module was located at the National Solar Thermal Test Facility (NSTTF) on a rotating platform that allows the collector to track the sun azimuthally, while the drive system of the module tracks the sun in elevation. Two axis tracking is not required but very useful in experimental studies when specific trough orientations need to

be studied. Figure 4 displays the LS-2 parabolic trough that was located at the NSTTF. Empirical data were collected from a similar trough for use at Sandia National Laboratories.

Figure 4. LUZ LS-2 parabolic trough at the NSTTF [3]

Parabolic troughs require accurate mirror alignment in order to maximize the solar energy output from the reflective surfaces onto the heat collection element (HCE). Therefore, it is necessary to determine accurate procedures and techniques to align the mirrors correctly and understand the impact of factors such as gravity on the techniques. Previous studies involving parabolic troughs used various innovative methods to determine the mirror angular displacements due to gravity. Luepfert et al. [4] used digital photogrammetry to digitally survey the reflective surfaces of a trough mirror module which gives highly accurate three dimensional coordinate data of the surface. This system required a high resolution camera and the procedure performed on a full scale model to properly evaluate the impacts of gravity deformation on the system. This data

was then processed to analyze the effects of gravity sag on the mirror beam quality. The slope deviations (slope errors) were determined from the coordinate data obtained from photogrammetry to evaluate the performance of the mirrors. Ulmer et al. [5] created a technique that evaluates the surface slope errors of parabolic trough collection systems by utilizing a digital camera and image analysis. Using the reflection of the HCE as a reference, a series of images are taken while rotating the trough, recording the appearance and disappearance of the HCE in the reflection. A computer program then evaluates the images to find the HCE reflections and draws lines that represent the upper and lower edges of the HCE reflection in the mirrors. The surface normals are calculated and yield the slope error angles as a consequence of gravity sag and manufacturing defects. This method needs a full size trough and a high resolution camera.

Diver and Moss [6] developed a technique (TOPCAT) to align parabolic trough mirrors using overlays of theoretical images of the HCE onto photographic images of the actual system to guide alignment. In this method, the collector is oriented at 0° (facing horizontally). Impacts of gravity sag on the mirrors and support structure in other orientations may affect the accuracy of this method. It is beneficial to use known gravity deformations to bias the alignment procedure to account for gravity induced deflections.

Gravity-induced bending and sag also affects characterization methods such as the Video Scanning Hartmann Optical Test (VSHOT). This method measures the local slope error distribution of a mirror facet in a particular orientation [7],[8]. The process works by utilizing a laser ray-trace on the reflective surface and taking high speed images of the collector to describe the characteristics of the surface of the collector. This method is quick, but again requires a full size prototype.

Lüpfert et al. [9] used a ray-tracing code and PARASCAN technology to evaluate the EUROTROUGH parabolic collector HCE intercept factor. Measuring the experimental solar flux distribution on the HCE with PARASCAN resulted in flux maps which could then be used to calculate the experimental intercept factor. Photogrammetry techniques were used to map the parabolic trough and then a ray-tracing code was utilized with these mapped models to evaluate the intercept factor of the system. This procedure quantifies the intercept factor of a parabolic trough which is the amount of energy present on the HCE divided by the total amount of energy being reflected from the collector. For an incident angle of 30° the PARASCAN and ray-tracing results were similar with intercept factor values of 0.964 and 0.965, respectively. This method shows that a ray-tracing model can provide accurate numerical results of trough intercept factors, but the deformed trough model was a result of scanning a full size trough system.

He et al. [10] utilized a Monte Carlo Ray Trace (MCRT) to evaluate the flux distribution on an LS-2 HCE. This method employs random photon movements and, at each reflection or transmission, determines whether the photon strikes the HCE. A mesh grid is created on the HCE to track the photon distribution along the tube. This information was then imported into FLUENT to analyze the outlet temperature of the working fluid through the tube. Using this method, the influence of geometric concentration ratios (GC) and different rim angles on the outlet temperature of the system were evaluated. As GC increased the outlet temperature increased. As the rim angle increased the heat flux on the tube decreased. The ray-trace was successfully employed to evaluate the effect on system performance when including the entire heat transfer process. In this process, intercept factors can be extrapolated from the heat transfer data.

However, this process fails to include any degradation to optical efficiency due to deformation of the collector surface.

In summary, several investigations into the impact of gravity deformations on solar collector efficiency have been focused on analyzing full scale trough systems. The need for a procedure to analyze gravity deformation impacts on the optical performance of design concepts before full scale prototypes is critical. The work presented here is unique because it couples FEA and ray tracing before a full size prototype exists. The coupling procedure can be used quickly and efficiently to evaluate many design concepts. This has the opportunity to aid in the way solar collectors are designed. This will result in cost-savings during the design stage, while also providing valuable information about system deformations when alignment procedures are performed.

The solar energy being emitted from the sun is a very important feature to the optical performance of all solar collectors. When the sun emits energy, the rays do not emit in a collimated way. In fact the sun shape causes rays to be emitted within a specific cone angle of ~0.55˚. The cone angle emission causes a beam spreading when solar rays reflect off of the solar collector mirrors. For example, a parabolic trough would reflect solar rays to a perfect focal line if the solar rays were exactly parallel to the normal to aperture of the collector. However, the cone angle emission causes a beam spreading effect so a beam spread image appears on the HCE and not on a perfect focal line. The solar energy being emitted within the cone angle does not have the same radiation intensity across the cone angle. The rays in the middle of the cone angle are at highest intensity and then the intensity drops off towards the outer rim of the cone angle. This effect is called sun limb-darkening. Figure 5 graphically represents the effect of the sun

limb-darkening across the sun cone angle. Further information on sun-limb darkening is available by Rabl [11].
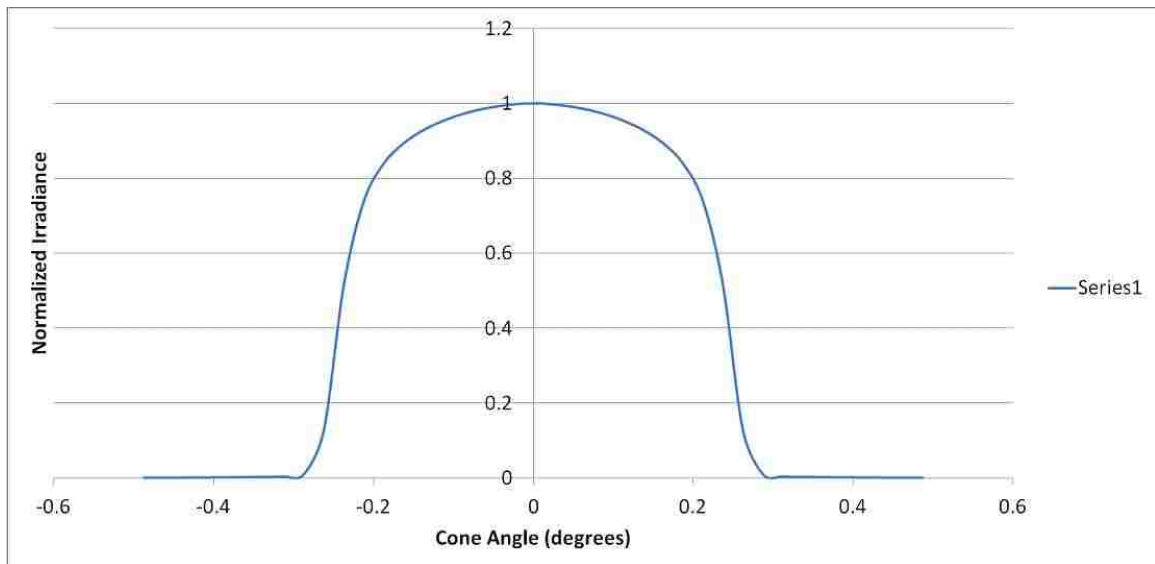
Figure 5. Sun limb-darkening of Normalized Irradiance versus Cone Angle [Data from 11]

3.   THEORY

The theory for the procedure being presented has two main analysis portions. The first portion is running Finite Element Analysis on the solar collector structure. Using FEA, the geometry is exposed to gravity loading and realistic structural boundary conditions. The deformed geometry information can be used to provide slope error maps of the deformations which is critical in understanding optical performance of a system. Physically, the collector reflective surfaces distort under loading which is characterized as a slope error. A slope error for this study is defined as the angular deviation of the surface normal vector of a finite element before and after loading. The surface normal of a finite element is known before loading and the new surface normal of that same element can be determined after loading. Thus, the slope errors of each finite element in

10

the system is determined and an accurate slope error characterization of the reflective surface can be shown. The FEA provides deformed geometry which is then imported into a ray trace program. A good reference for using FEA in mechanical engineering design is by Mottram and Shaw [12]. Mottram and Shaw describe the mathematics behind choosing types of mesh elements, logical simulation steps, and post-processing of information. Other literature focused on structural analysis of solar collectors is provided by Moya et al. [13] and by Dunder [14]. These studies focus on the structure of collectors under various operating and loading conditions.

The ray trace program applies the critical physical properties to the deformed collector surfaces. The ray trace can provide accurate flux maps, ray trace statistics, and most importantly, determine beam quality due to gravity loading. The surface slope errors and beam quality is known and from this information design changes can be employed to improve the optical performance of the solar collector. An in depth ray tracing analysis description is provided by Welford and Winston [15]. They approach ray tracing in a solar energy context which is helpful for understanding this analysis. An example of using optical equations to solve for optical performance of trough models is detailed by Eames et al. [16]. This model evaluates a two-dimensional analysis using numerical techniques to solve heat transfer and optical performance equations. A study evaluating the finding of intercept factors for parabolic troughs is detailed by Kalogirou et al. [17]. Several different methods are compared here and can be referenced for a deeper understanding of other ways intercept factors are found.

4. SOFTWARE

Two programs are involved in the procedure being developed within this study. SolidWorks is the chosen Computer Aided Drafting program (CAD) with its internal Simulation feature being used as the FEA program. APEX is the ray tracing program used in this study. ASAP is another ray tracing program which is well established and will be used to verify results from the APEX program.

4.1 Solidworks and Solidworks Simulation

SolidWorks is a well-known and respected Computer Aided Design (CAD) program. It has emerged as an industry leader. It has a very strong presence in current engineering college programs which makes it a perfect software for the FEA and ray tracing coupling procedure presented here. The reason for choosing this program is that it is intuitive to use, accurate, and most engineers have already been exposed to it.

SolidWorks Simulation is the FEA program embedded within SolidWorks. Having an embedded FEA program makes the transition from geometry to FEA analysis very simple. The material properties assigned in the CAD program are retained simplifying the finite analysis procedure. SolidWorks has done a good job in coupling the CAD features to the FEA features. This FEA program has a high learning curve making it a very suitable program to incorporate into this procedure for analyzing solar collectors.

4.2 APEX

APEX is a fairly new ray-tracing program available commercially today. It is produced by Breault Industries which is a renowned company for optical modeling software. It was chosen to be the ray tracing program for this analysis because it is also

embedded within SolidWorks. This makes the use of the program very simple with a fast learning curve. With most engineers already fluent with SolidWorks, this program can be easily learned. The CAD geometry needed for ray tracing is available directly from SolidWorks and SolidWorks Simulation. APEX is a suitable program for the ray tracing portion of this solar collector analysis.

4.3 ASAP

ASAP is a well-known ray tracing program developed by Breault Industries. It has been used repeatedly by scientists and engineers for optical modeling projects. This program is the "older brother" of APEX. Results from APEX are validated against ASAP to verify that APEX is producing quality optical results.

4.4 Microsoft Excel

Microsoft Excel is a well known data analysis tool used by many engineers. It has many capabilities and is used for post-processing the FEA and ray trace results. Excel is capable of providing slope error characterization plots and makes analysis of the many data points very easy.

4.5 MATLAB

MATLAB is a mathematical analysis tool available to many engineers. It has programming abilities which aid in the post-processing of data. It is used in conjunction with Excel to quickly and accurately post-process data. It is mainly used for manipulation of large matrices and also provides some slope error characterization plots. MATLAB was easier to use in terms of manipulation of plots. The color scales and axes are easier to adjust compared to Excel.

5. PROCEDURE

The procedure for analyzing solar collectors is composed of two main parts. The first portion consists of creating the geometry of the collector and performing the FEA necessary to determine the gravity induced deformations on the system. The second portion consists of importing the deformed geometry into the ray trace program and determining the optical performance of the gravity deformed collector.

5.1 Finite Element Analysis

The Finite Element Analysis is used to characterize the deformations of the solar collector reflecting surfaces. A single LS-2 parabolic trough is used as an example of the procedure. Initially, only a single mirror column is being demonstrated for procedure simplicity. However, results for a full trough module will be shown in Section 6. Note that this analysis has been developed so that it can be used for any solar collector.

5.1.1 Finite Element Metrics and Terms

A displacement is defined as the translation and rotation of an FEA element from its original location after loading. This is reported in three dimensions using a standard length unit such as millimeter or inch. The term deformation is also used to describe displacements.

A slope error is defined as the angular deviation of the surface normal vector of a finite element before and after loading. The surface normal of a finite element is known before loading and the new surface normal of that same element can be determined after loading. A slope error is commonly used to describe the optical accuracy of a reflecting surface. A perfectly reflecting surface wouldn't have any slope errors. Slope errors occur

from loadings, but there are inherent mirror inaccuracies induced during manufacturing and assembly processes which also cause slope errors to be present.

5.1.2 Geometry

The dimensions of the modeled system are based upon measurements taken of the LS-2 module at the NSTTF. The measurements of small features were recorded using a digital caliper (tolerance of 0.0254 mm), and large features were recorded using a measuring tape (tolerance of 2.54 mm). All of the measurements of the trough had to be completed in person. The geometry CAD drawings were not available for modeling purposes. When modeling this caused some parts to not align correctly with their conjugate pieces. Thus, some engineering judgment was used to get the CAD geometry to "fit" correctly. SolidWorks requires parts to accurately match in order for the parts to be mated correctly, such as in the case of coincident features.

The full collector system was modeled using two main assemblies. The first assembly will be the one be demonstrated for example of the procedure. The second assembly includes the rest of the parabolic trough structure for which only results will be shown for. The first assembly is composed of the mirror panels with the brackets and trusses attached to them. The contoured mirrors for the parabolic trough were created using extruded parabolic sketches and mirroring symmetric parts. The dimensions of each mirror in the assembly were approximately 1.57 m x 1.31 m for the two outer mirrors and 1.57 m x 1.39 m for the two inner mirrors. All mirrors have a thickness of 4 mm. There are two bracket types used for joining the mirrors to the support structure. A hinged-pin bracket allows for the mirror to be aligned while a fixed bracket supports one end of each mirror. A fixed bracket is rigidly attached to the mirrors. The truss support structure is

composed of hollow rectangular tubing. The brackets and truss support were given material properties of AISI 304 steel with the default material properties being included within SolidWorks.

The assembly contains many different parts which are then mated together to form a single cohesive geometric system. It is crucial to understand the mating types needed in the geometry in order to the system to behave correctly during the FEA portion of the analysis. Coincident mates will bond surfaces together unless otherwise specified during analysis. Concentric mates concentrically mate circular features together. However, the concentric mating does not allow for rotation about the circular features during analysis. In order to have parts rotate during FEA, a mechanical hinge mate must be used. This is required for this particular trough system as seen in Figure 6. The mirrors are supported on the structure using two fixed brackets and two hinged brackets. The hinged brackets allow the mirror to rotate around a pin so that the mirrors can be aligned to the line focus point required. The hinged mate was used for mating the hinged brackets to the mirror support structure. The first assembly will be the one be demonstrated for example of the procedure. The second assembly includes the rest of the parabolic trough structure which has results presented in Section 6 of this report.

Fixed Bracket
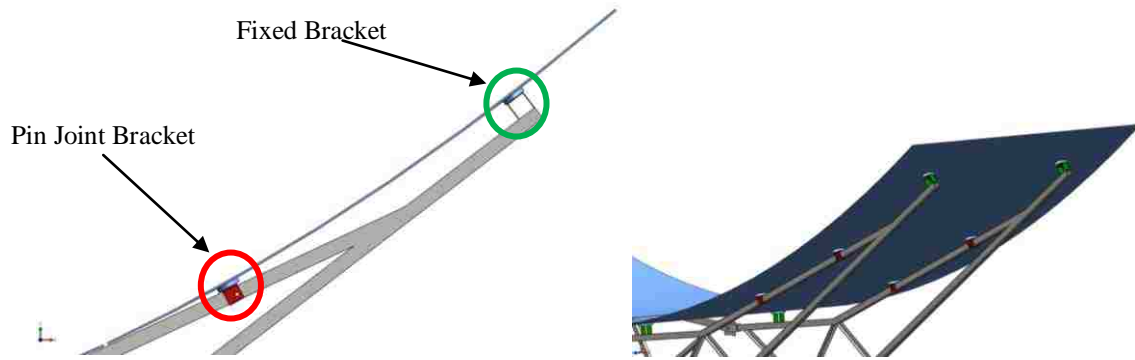
Pin Joint Bracket

Figure 6: Parabolic trough truss to mirror brackets, Red brackets signify pin-joint brackets, Green brackets represent fixed brackets, (Left) Side View of Outer Mirror, (Right) Isometric View of Outer Mirror

The second assembly is the main assembly for the full trough collector. It includes the complete parabolic trough structure including the torque tube, mirrors, trusses, left/right ground supports, and heat collecting element with supports. The first assembly is copied five times in this assembly to replicate the five mirror columns present on an actual trough module. Each of the mirror columns is mated to a torque tube. The torque tube is rotated to allow the trough to track the sun throughout the day. The tube is a circular hollow tube with a quarter inch wall thickness. The actual wall thickness was not known and could not be directly measured, but this thickness was deemed appropriate using engineering judgment. The torque tube was attached at either end by a ground support which supports the entire trough. It was attached using an "adapter" plate which connects the torque tube rigidly, but still allows for rotation about the end ground supports. The supports are made from L-channel weldments for the cross supports and hollow rectangular tubes for the main support frame. The heat collecting element (HCE) is composed of a glass envelope which surrounds a thermal absorber. There is a vacuum gap between the glass envelope and absorber to prevent convective heat transfer. The

HCE is held up by simple V-shaped supports extending from the torque tube. The final model is shown in Figure 2 when compared to the actual trough system. The SolidWorks model has the ability to rotate about the torque tube axis. This means the trough can be rotated to track the sun in elevation.

Figure 7. (Top) Photograph of actual LS-2 trough [3]; (Bottom) SolidWorks® model of LS-2 trough.

5.1.3   Finite Element Analysis Setup

The finite element simulations for an example of this procedure are focused on a single four-mirror column. Each column of mirrors on the LS-2 is attached separately to the torque tube. Therefore, deflections caused by gravity-induced bending of the mirrors and support structure (trusses and brackets) in different orientations can be simulated independently for individual columns (i.e., bending of mirrors and supports in one column does not affect the bending of mirrors and supports in another column). The single column of mirrors is simulated using finite element analysis in SolidWorks Simulation to obtain the deflections on the reflective surface of the mirrors. The single mirror column was subjected to gravity loading with restraints placed on the truss supports corresponding to the actual restraints. The restraint was a fixed condition which

is accurate to having the truss support being rigidly fixed to the torque tube (Figure 8). The fixed restraint does not have any degrees of freedom especially since there is not a torque tube displacement.
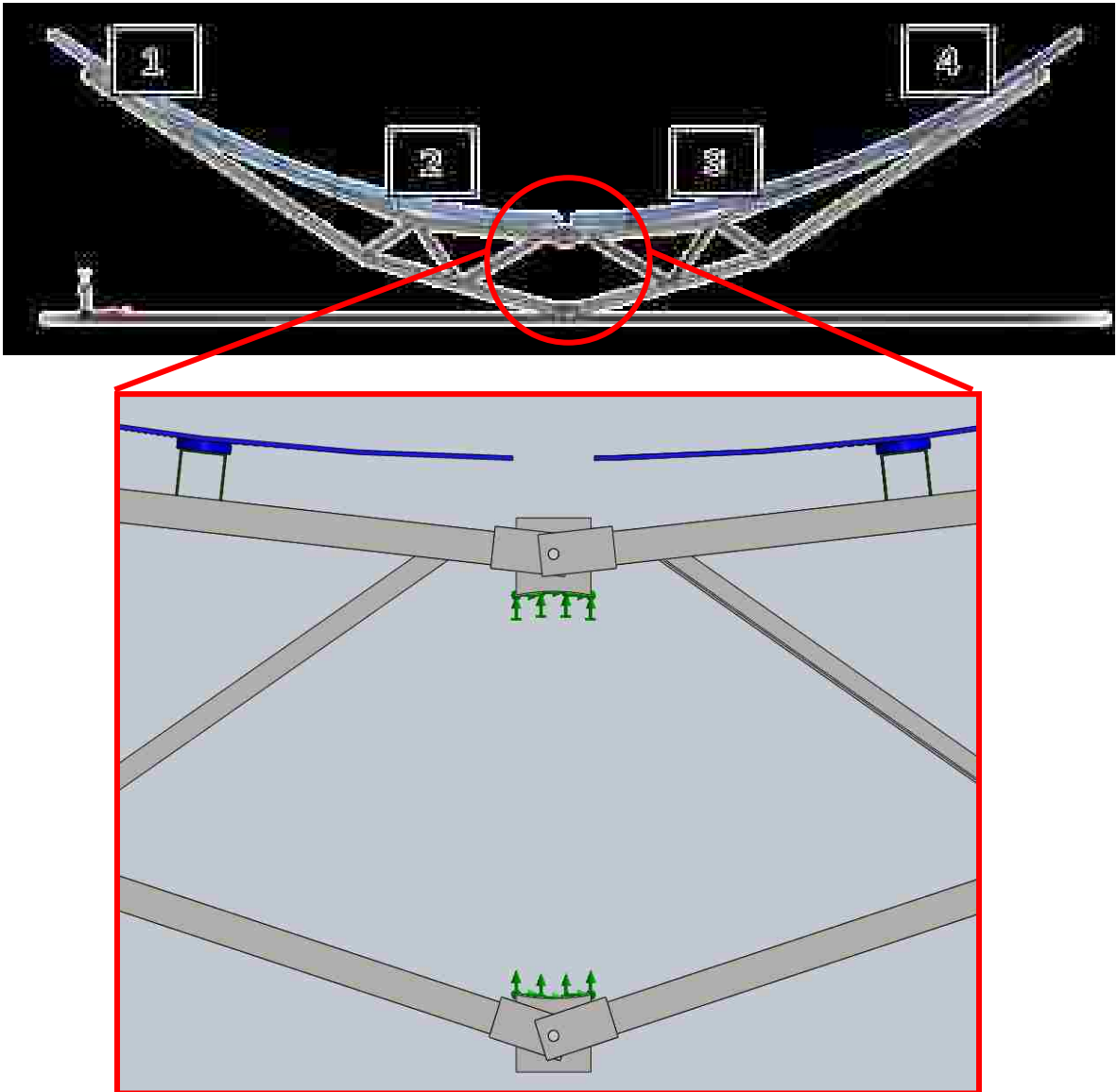
Figure 8. Fixed restraints placed on single mirror column for FEA simulation

In this study, solid mesh elements were used to accurately portray the connections between the mirror and the truss structure. A solid mirror allowed for easy attachment of the truss to the mirrors through the use of simple brackets and as a result the bonding

19

conditions were accurately portrayed during simulation. An alternative study was

performed utilizing shell elements on the mirror panels, but in some of the studies it was

concluded that the bonding conditions were skewed and mesh continuity was problematic

between the brackets and mirrors. These conditions were providing abnormal results

compared to the solid model at the boundary conditions of the brackets, therefore a

purely solid element mirror module was utilized. For solid meshing elements in

SolidWorks, the elements are tetrahedral 3D solid elements for each component. Each

element is composed of 10-nodes which allows to for more accurate solution

interpolations. The following mesh settings were chosen to perform the FEA for this

solar collector single mirror column:

1. Global Element Size = 1.03968 in

2. Mesh Controls (specified mesh element sizes for specific parts)

    a. Brackets = 0.3182 in

    b. Mirror Truss Supports = 0.636417 in

    c. Torque tube mounting plates = 0.39776 in

The mesh controls are necessary because small parts cannot be meshed with the

specified global element size. A mesh control allows small parts to be meshed with a

suitable element size.

The final mesh took less than five minutes to complete and the total simulation run

time was around an hour for a very fine mesh. A coarser mesh took under half an hour

but provided less accurate displacement results. A grid-independence study was

performed to make sure that the solution from the FEA is not grid dependent. The

number of elements was recorded as the mesh is refined and then the corresponding

maximum displacement in the model was analyzed for each mesh refinement. The appropriate mesh size was chosen after the maximum displacement in the model differed by less than 0.5% at least. The chosen mesh element sizes were considered accurate once a grid-independence study was performed.

The analysis was run in two main positions, each proven to be mesh independent. The first position is the 90° position (reflective surfaces facing upward) and the second position is the 0° position (reflective surfaces facing horizontally). Figure 9 illustrates the mirror positions and mirror labels used in the simulations. The trough column had an identical mesh for each position identified. This guarantees that each position can be compared against each other without concern about mesh differences, i.e. the FEA elements are labeled the same such that the elements from each loading position can be directly compared. Although the 0° position is shown rotated in Figure 9 and throughout the rest of this study, the global coordinates for each node are the same as those in the 90° position. The FEA boundary conditions are rotated such that the proper orientation is achieved to study the effects due to gravity. Each of the mirrors is assigned a number label such that each mirror can be uniquely identified during the analysis process. The labels were arbitrarily chosen.

The displacement induced by gravity in these two trough orientations are reasoned to produce the largest displacements in the mirrors. In the 90˚ position, the mirrors would be "flattened" out by gravity. In the 0˚ position, the mirrors would be "folding" in on themselves. These effects will cause the greatest displacements in the mirrors due to gravity. Using these two positions a threshold approach to this problem setup is introduced. It is reasoned that these two positions could cause the greatest decrease in

intercept factor and would be the best models to identify any degradation in optical performance. Also, when designing structures it is useful to identify the largest displacements in the structure and mitigate these. In this procedure, a detailed map of the slope errors in the mirrors could provide valuable insight into the structural design of the system. Thus, the maximum displacements due to gravity loading is seen as most useful in this problem setup.
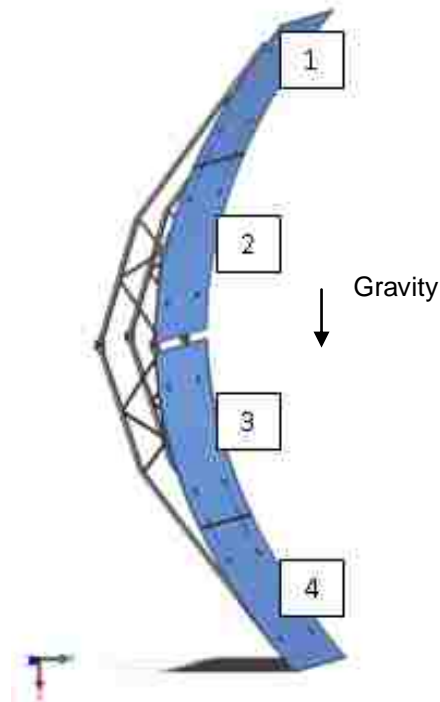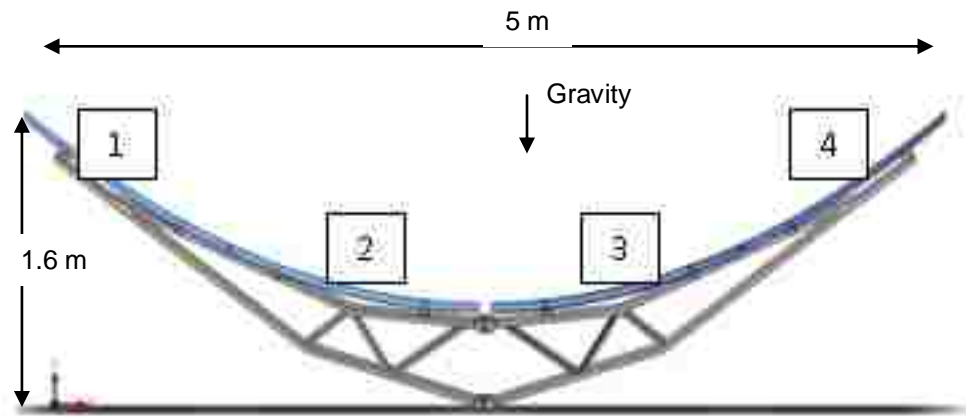
Figure 9. (Top) 90° positioned trough model with labeled mirrors, (Bottom) 0° positioned trough model with labeled mirrors.

The mirrors had direct interactions with the truss support system through a series of brackets causing specific boundary conditions to be placed on the model in order to get accurate simulation results. Two of the four brackets which connect each mirror to the truss are fixed to the mirror and truss which is provided in SolidWorks by a simple

bonded connection provided from the coincident mate between the components. The coincident mate is automatically considered as global contact between components when the model is imported into SolidWorks Simulation. The other two brackets are hinged on the mirror through a pin support system so that the mirror is free to rotate about these pins. In order for Simulation to recognize these pinned boundary conditions between the mirrors and truss, a special mate had to be applied to the bracket/mirror component interactions. A hinge mate allows for the mirror to rotate about the pin support and allows the realistic movement of the system to be simulated in the FEA. The entire model is required to be fixed using a fixed geometry restraint to allow the simulation to have a point of reference. Fixed geometry boundary conditions were applied to the surface on the truss-to-torque tube mounts where the torque tube is normally attached. These boundary conditions allow the model to be stabilized and proper analysis to be performed.

The only load in this analysis is gravity. In the 90° position, gravity is normal to the center of the trough center line. For the 0° position, the gravity vector was simply rotated from the 90° trough position by 90° rather than changing the orientation of the actual geometry. Gravity is set to a value of 9.81 m/s^2, but the direction changes according to the model. In the 0° position, gravity was -9.81 m/s^2 in the Y-direction. In the 90° position, gravity was 9.81 m/s^2 in the X-direction. The coordinate system was chosen such that the Z-axis runs parallel to the torque tube axis for the mirror column.

5.1.4   Finite Element Analysis Results

The results discussed in what follows were taken directly from SolidWorks. The displacement figures are exaggerated so that the deformations can be easily seen. The original mirror location is transparent on the displacement figures for reference.

Figure 10 illustrates the displacements of the mirrors during gravity loading in the 90° position. The maximum displacement occurs on the edges of the outer mirrors with a value of ~0.9 mm. As can be seen, mirrors 1 and 4 open outward from the center of the trough when compared to the original shape, which can be seen as a transparent image in Figure 10. Figure 10 has a deformation exaggeration scale of 200 applied to it so that the displacements can be visualized (which is why the trusses appear to come through the deformed mirrors). The trusses are much more rigid than the mirror structures given the appearance that they did not deform much, but they deform a slight amount under gravity loading. The truss displacement results are not shown explicitly here because the mirror displacements are key to the procedure, but will be shown in Section 6 for the full trough module.
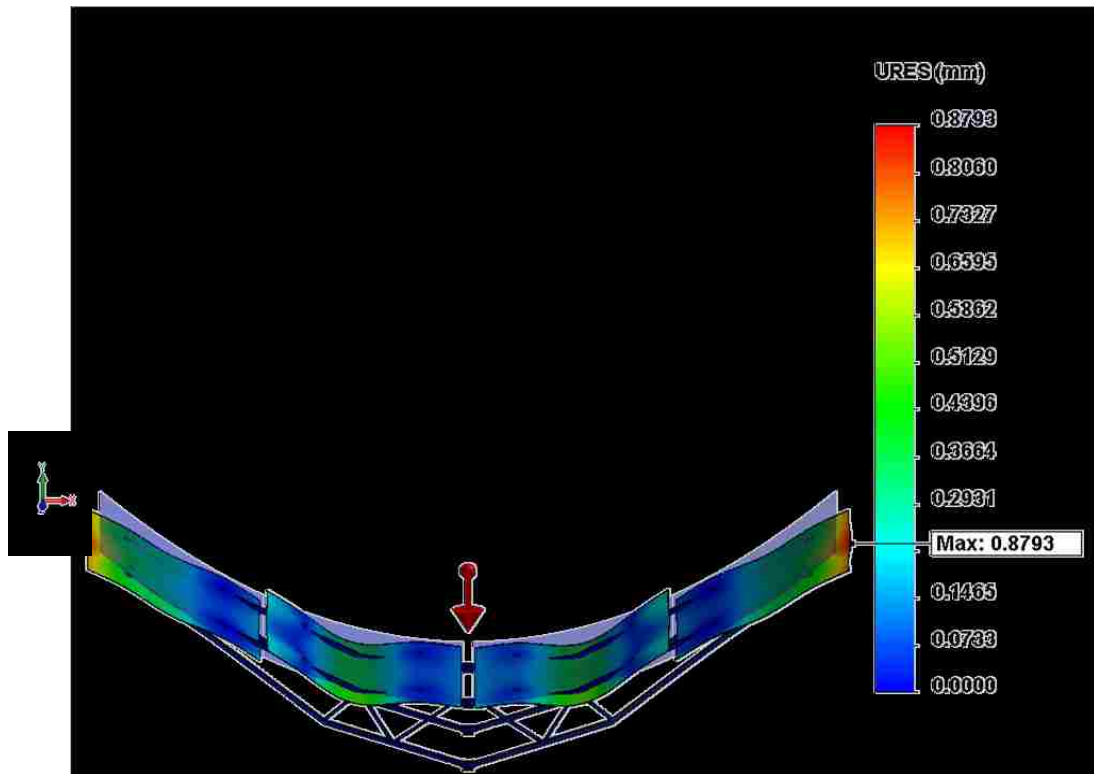
Figure 10. 90° position displacements after gravity loading with transparent original shape (exaggeration scale = 200).

Figure 11 displays the mirror displacements in the 0° position. The maximum displacement occurs along the edges of the outer mirrors with a value of ~0.7 mm. The top of the trough bends downward toward the center of the trough, while the bottom mirror tilts downward as well. Figure 11 has a deformation exaggeration scale of 200 (which is why the trusses appear to come through the deformed mirrors).

The support structure for the mirrors (trusses and brackets) contributed to the overall displacements of the mirrors. The amount of displacement caused by bending of the support structure ranged from ~1.5-4.0 times the displacements caused by individual mirror deformations alone, depending on the mirror positions. In the 90° position, mirrors 2 and 3 experienced about a 1.5x increase of deformation due to the supports.

Mirrors 1 and 4 experienced a 4x increase in deformation. In the 0° position, mirrors 2 and 3 exhibited about a 2x increase in deformation while mirrors 1 and 4 showed about a 3.5x increase.
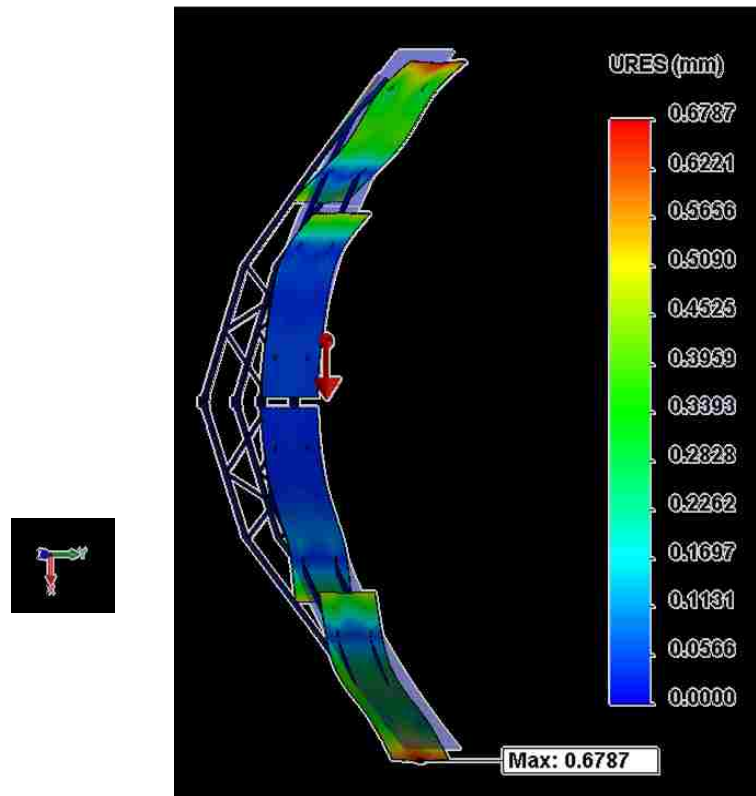
Figure 11. 0° position displacements after gravity loading with transparent original shape (exaggeration scale = 200).

5.1.5 Slope Errors

Although only two positions of the mirrors were analyzed, there were three slope-error studies performed. The first case explored the gravity-induced displacements and resulting slope errors of the mirror column positioned at 90° relative to its undeformed shape at 90°. The second case examined similar displacements and slope errors in the 0°

position. The third case examined the slope errors resulting from the deformed shape in the 0° position relative to the deformed shape in the 90° position.

To determine the slope error distribution of each mirror on the single trough column, the following procedure was followed. The first step was to record the nodal positions of the reflective surfaces based on the undeformed shape of the model. Each node is specified by x, y, and z coordinates, and these values are recorded for the top reflective surface of the mirrors. After simulating the gravity-induced bending of the mirrors and support structure, the nodal coordinates and displacements from their original position are recorded and imported into a Microsoft Excel spreadsheet for each individual mirror.

The nodal coordinates and displacements of the deformed and undeformed shapes are used to calculate unit vectors for adjacent nodes, and these vectors are used to determine rotations (slope errors) about the z-axis, which is parallel to the HCE tube, as follows. First, two vectors were identified between adjacent nodes on the model. The first vector is composed of two coordinates from two adjacent nodes on the undeformed shape's reflective surface. The second vector is composed of the displaced coordinates (after deformation) of the same two nodes as used for the first vector. These two vectors intersect each other and the Θ between the two intersecting vectors is the angular displacement. Figure 12 describes the process.

The second step is to translate the second vector (created from the deformed shape's nodes) so that its first point is coincident with the first point of the first vector (undeformed shape's nodal vector). This also translates the second point of the deformed shape's vector. Figure 12 describes the process.
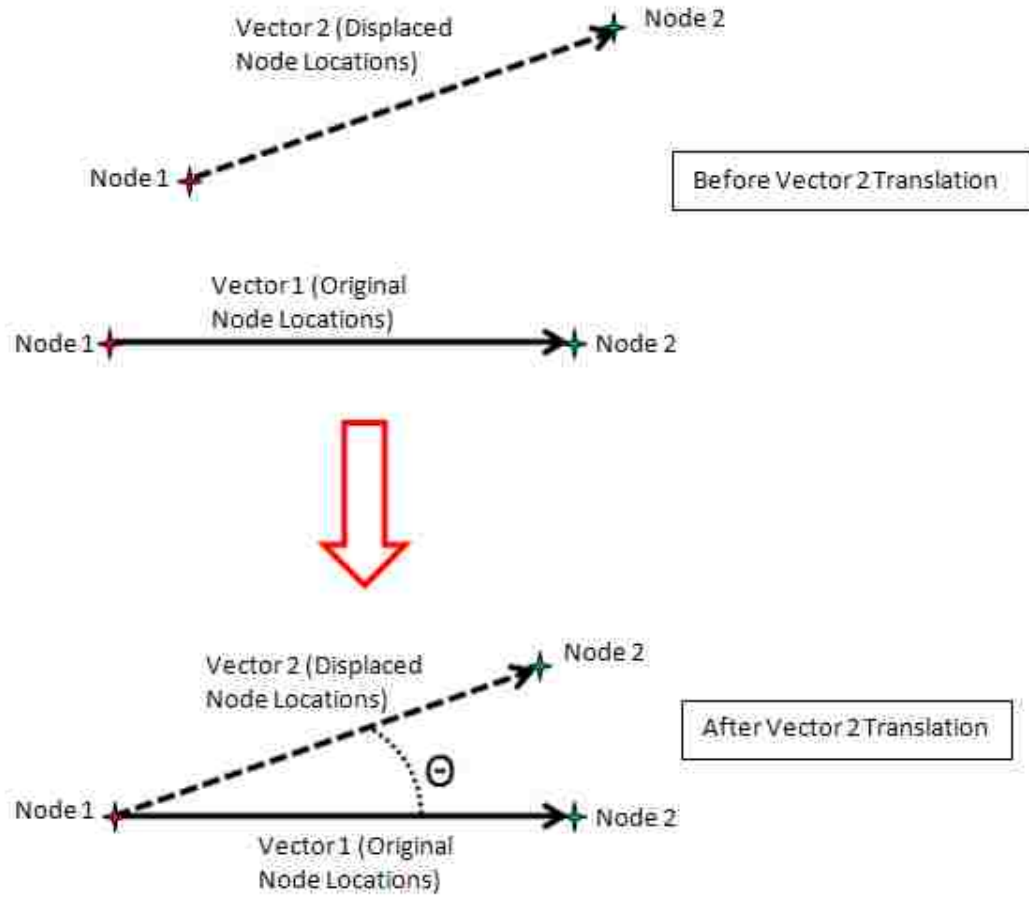
Figure 12. Finding the slope errors from the FEA, Steps 1 and 2 in finding the slope errors

The final step is to determine the angle, Θ, between the two vectors. The dot product is used to find the angle according to the formula: $A \cdot B = |A|*|B|*\cos\Theta$, $A/|A|$ is the unit vector of the first vector (undeformed shape) and $B/|B|$ is the unit vector of the second vector (deformed shape). The direction of the angular rotation can be determined from the cross product of the two vectors found above. Only rotation about the z-axis was considered. If the z-component of the cross product was negative (into the page in Figure 9), then that local section of the mirror rotated clockwise. If the z-component of the cross product was positive (out of the page in Figure 9), then that local section of the mirror

rotated counter-clockwise. These signs were then applied to the corresponding slope error values.

The inputs required for finding the slope errors are taken from Simulation. The first required input are the coordinates of the surface element nodes before deformation occurs. Each mirror surface was probed in SolidWorks. The probing gives the node coordinates of each surface element before gravity deformation. The second required input is the coordinates of the displaced nodes. Unfortunately, SolidWorks does not provide a simple way to extract the displaced nodal coordinates of the mirrors. However, SolidWorks does provide the displacements in the X, Y, and Z directions. The displacements in these coordinate directions were extracted and then added to the original nodal coordinates.

The coordinates were imported into the slope error calculator created within Microsoft Excel. Custom Visual Basic macros were written to automate the functions required to calculate the slope errors. MATLAB was used as a supplemental tool to quickly generate the slope error plots representing the slope error distributions of the mirrors.

Table 1, Table 2, and Table 3 contain the statistical values of the slope error data that were found for each case. Slope error values are plotted in Figure 13, Figure 14, and Figure 15 with the values assigned a color depending on its magnitude. Figure 13 and Figure 14 of the slope error figures have a color bar that range from +3 mrad to -3 mrad, with red denoting a positive (counterclockwise) rotation and blue denoting a negative (clockwise) rotation about the z-axis (parallel to the HCE tube). Figure 15 has a color bar ranging from +3.5 mrad to -3.5 mrad. It should be noted that in order for the plots to be

created, only every third value was plotted. This method allowed the plot to be generated and manipulated efficiently while still giving an accurate visual representation of the slope errors.

Table 1. 90° position slope error statistical values of all elements present on each mirror surface

All Units in Milli-radians (mrad)				
	Mirror1	**Mirror2**	**Mirror3**	**Mirror4**
Max	1.852	2.002	2.133	1.651
Min	0.000	0.001	0.000	0.000
Average	0.668	0.840	0.878	0.668
Median	0.636	0.749	0.806	0.649
St. Dev.	0.409	0.472	0.475	0.391

The slope error values for the 90° position indicate that the maximum absolute slope error is found in mirror 3 which is about 2.133 mrad. Mirror 3 has the highest average absolute slope error of 0.878 mrad.

Figure 13 illustrates the slope errors for the 90° position trough. The slope errors are relatively consistent with intuition. As expected, when the trough reflective surfaces are in the 90° position, the trough is expected to open up with the mirrors rotating away from the trough center. Mirror 1 has red at its far left edge indicating that the slope error is positive and, therefore, rotated in the counterclockwise direction. Mirror 4 has blue at its far right edge indicating the rotation about the z-axis is in the clockwise direction. The magnitude of the slope error values are nearly symmetrical for opposing mirrors (i.e., Mirror 1/Mirror 4 and Mirror 2/Mirror 3). The reason they are not identical is due most likely to un-identical mesh element patterns applied to each mirror. This is hard to control in SolidWorks since most of the meshing operations are automatic. A differing mesh pattern will result in slightly different results for the opposing mirrors. However, the average slope errors and standard deviations are are near identical.

90degree vs. Undeformed Position All Mirrors: Slope Errors (Units in mrad)
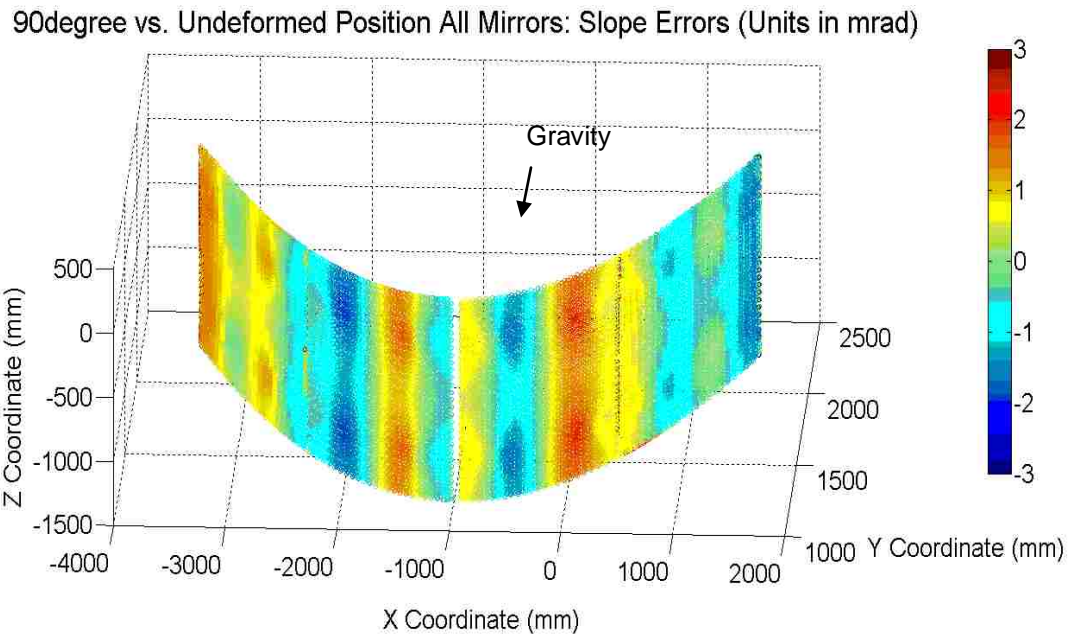
Figure 13. Simulated slope errors (angular rotation about the z-axis parallel to the HCE tube) for the 90° vs. undeformed case. Positive values indicate counterclockwise rotation, and negative values indicate clockwise rotation.

Table 2 displays the slope error values when the trough was in the 0° position. The slope error values for the 0° position indicate that the maximum absolute slope error is found in mirror 1 and 4 with a value of 2.377 mrad. Mirror 1 has the highest average absolute slope error of 0.914 mrad.

Table 2. 0° position slope error statistical values of all elements present on each mirror surface

All Units in Milli-radians (mrad)				
	Mirror1	**Mirror2**	**Mirror3**	**Mirror4**
Max	2.377	2.003	1.982	2.377
Min	0.000	0.000	0.000	0.000
Average	0.914	0.464	0.461	0.900
Median	0.947	0.214	0.218	0.933
St. Dev.	0.588	0.586	0.572	0.581

Figure 14 illustrates the slope errors for the 0° position. The figure is oriented the same as in Figure 13 for easy comparison, but the actual configuration would have the column of mirrors rotated clockwise by 90°. At mirrors 1 and 4, the slope errors along the outer edges are negative, indicating that the ends are rotating clockwise (sagging downward) due to gravity-induced bending. The middle mirrors (2 and 3) have much lower slope errors.
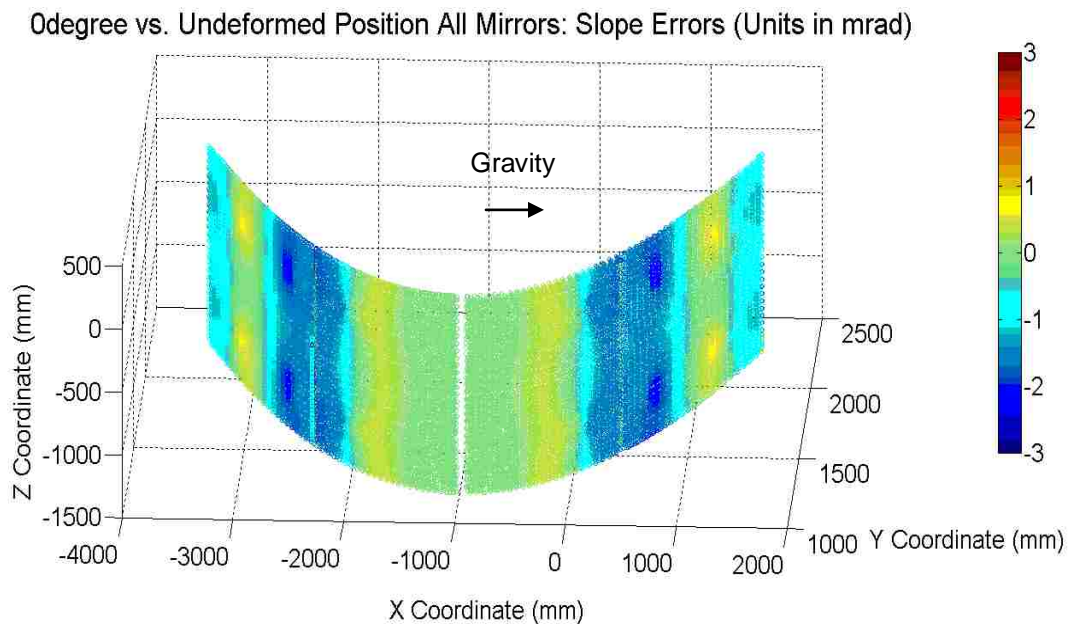
Figure 14. Simulated slope errors (angular rotation about the z-axis parallel to the HCE tube) for the 0° vs. undeformed case. Positive values indicate counterclockwise rotation, and negative values indicate clockwise rotation.

Table 3 displays the slope error values resulting from a comparison of the deformed trough in the 0° position relative to the deformed trough in the 90° position. In other words, the slope errors (angular rotations) of mirror elements are calculated when the trough is rotated from the 90° position (facing upward) to the 0° position (facing horizontal), where gravity is included in both positions. The slope error values for the

90° position versus 0° position indicate that the maximum absolute slope error is found in mirror 3 at 3.344 mrad. The highest absolute average slope error is found in Mirror 1 at 1.304 mrad. These results indicate that a rotation of the trough from 90° to 0° can yield effective slope errors on the order of 1 mrad due to gravity bending when considering the slope errors in both positions.

Table 3. 90° versus 0° position slope error statistical values of all elements present on each mirror surface

All Units in Milli-radians (mrad)				
	Mirror1	**Mirror2**	**Mirror3**	**Mirror4**
Max	3.237	1.922	3.344	2.594
Min	0.000	0.000	0.000	0.000
Average	1.304	0.773	1.260	0.818
Median	1.222	0.753	1.110	0.468
St. Dev.	0.785	0.437	0.848	0.743

Figure 15 illustrates the slope errors of the 90° versus 0° positions. At the edge of mirror 1, the slope errors are negative (clockwise rotation). This is consistent when analyzing the 90° and 0° positioned mirrors. When the trough is rotated 90° clockwise from the face-up position, mirror 1 will rotate clockwise. Initially, in the 90° position, mirror 1 is sagging outward from the center (see Figure 4). After rotating it to the 0° position, mirror 1 sags downward toward the center of the mirror (see Figure 5). The result is a large clockwise rotation along the outer edge of mirror 1. For mirror 4, the gravity induces a sag outward from the center in both the 90° and 0° positions. Thus, the rotation (slope error) of mirror 4 is less than mirror 1. Parts of the two inner mirrors (2 and 3) also show fairly significant slope errors as a result of the trough rotation.
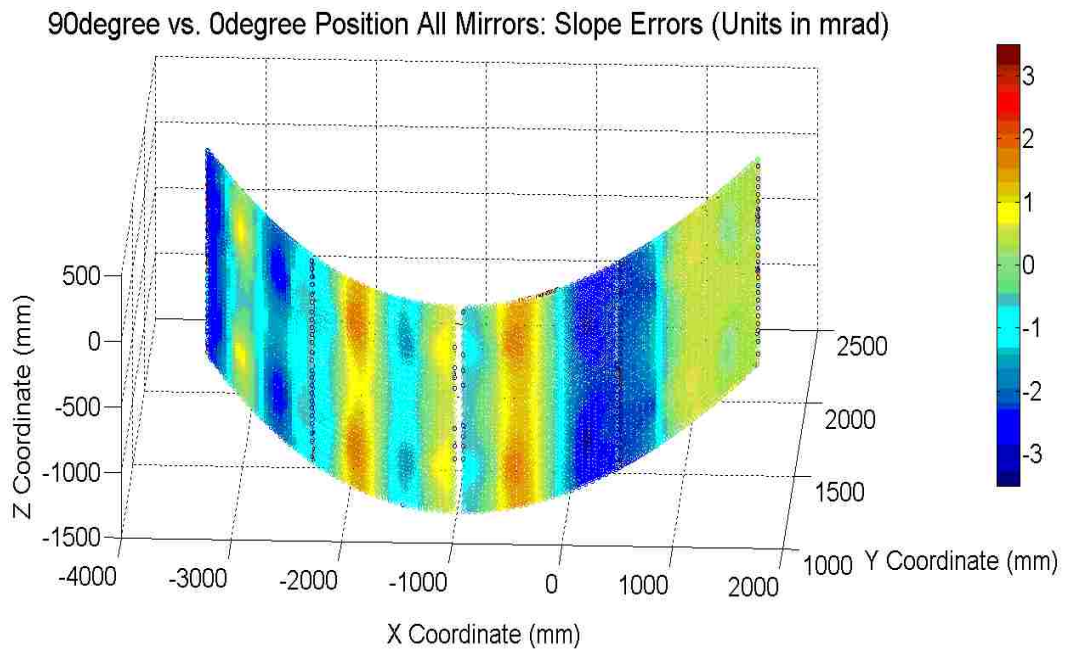
Figure 15.Simulated slope errors (angular rotation about the z-axis parallel to the HCE tube) for the 90° vs. 0° case.   Positive values indicate counterclockwise rotation, and negative values indicate clockwise rotation.
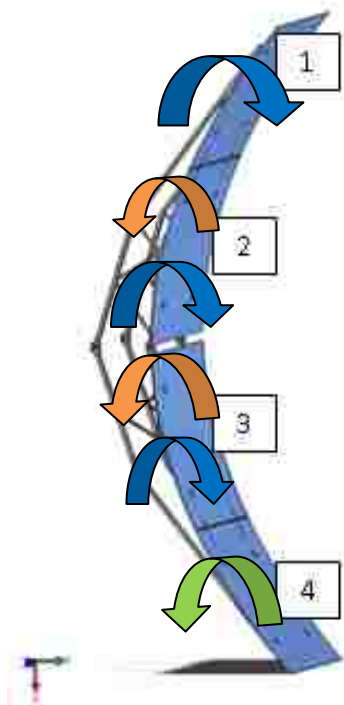
Figure 16. Schematic indicating the slope error rotations caused by rotating the trough column from the 90 degree position to the 0 degree position, arrows indicate clockwise or counterclockwise dominant rotations about the z-axis

Diver et al. [6] noted that during testing TOPCAT Alignment mirror alignment techniques on the SEGS LS-2 at the NSTTF, slope errors of 2 mrad could be detected. The study performed had the trough in the 90° position and this observation can be directly related to the 90° position study done by FEA in this study. As can be seen in Table 1, the maximum slope errors calculated in the model were 2.133 mrad which is close to those observed by Diver. Wendelin [7] performed slope error analysis on a Solargenix trough module using VSHOT characterization techniques and determined that maximum slope errors could peak at about 5 mrad, but from the slope error plot it appears as if the nominal slope error value for this system is about +/- 3 mrad. The +/- 3 mrad range closely corresponds to the slope error findings using FEA analysis even though the trough module studied by Wendelin was not exactly identical to the LS-2.

36

Ulmer et al. [5] study of a EuroTrough four mirror module using reflection method resulted in large maximum slope errors at very select spots on the model. However, generally the facets produced high slope errors of about +/- 4 mrad in all four mirrors. The slope error plot shows that many spots of the mirrors have slope errors of +/- 2 mrad. The FEA analysis provided slope errors of +/- 2 mrad and lower which corresponds to the Ulmer study.

5.1.6 Finite Element Analysis Conclusions

Finite-element modeling was performed on the LS-2 parabolic trough solar collector in order to determine the effects of gravity sag on the mirror facets. The displacements were calculated for each mirror and then analyzed resulting in a distribution of slope errors along the mirror. The slope errors resulting from gravity-induced bending of the mirrors and support structure were as high as ~2 mrad, depending on the location of the mirror facet on the collector. The slope errors resulting from a change in orientation of the trough from the 90° position to the 0° position with gravity were as high as ~3 mrad, depending on the location of the facet.

These results indicate that gravity-induced bending of the mirrors and support structure can have a significant impact on the optical quality of the collector. Characterization and alignment methods that measure the optical quality of collectors in a particular position (e.g., 0°) need to consider these effects to ensure accurate characterization and alignment when the collector is positioned in other orientations. The results of these simulated deformations and slope errors will be used in a ray-tracing code to determine the impact of gravity loading on HCE intercept factors in future work.

Unfortunately, actual displacement measurements were unable to be taken due to disassembly of the trough at the NSTTF. However, other studies have shown that SolidWorks Simulation analysis can provide results close to experimental data. Moya et al. [13] performed an analysis between a heliostat empirical displacement data and FEA with accurate results. This gives confidence that the modeling approach for the trough would yield similar results to empirical trough data if any were available.

5.2   Ray Tracing Analysis

5.2.1   Ray Trace Analysis Metrics and Terms

For a parabolic trough the intercept factor is the main optical performance metric. An intercept factor is the ratio of actually energy on the heat collecting absorbing element to the total energy reflecting from the collector surface. A perfectly reflecting solar collector without deformations will result in an intercept factor of 1 since all of the energy reflecting from the collector surface will impact the HCE absorbing element. Other collector systems such as heliostats rely on flux maps and beam shape to quantify optical performance. These metrics are easily found using plane targets during ray tracing.

An incident angle is the angle between the normal of the collecting surface to the aperture and the incoming solar rays. This angle is used to evaluate solar collector performance when tracking the sun throughout the day. It is expected that a larger incident angle results in more energy missing the HCE resulting in a lower intercept factor.

An incident angle modifier accounts for deviations from a zero incident angle between the sun and the collector for experimental studies. It is defined as the efficiency

38

of the trough at any incident angle to the sun divided by the efficiency of a trough at zero incident angle to the sun.

When a source is set to emit photons (a ray), the photon is emitted within a defined solid angle (cone angle). An apodized source means that the intensity of the energy leaving the source in a ray is non-uniform along the defined emitting cone angle.

5.2.2 General Ray Trace Information

The finite-element models were used to determine the impact of gravity loads on displacements and rotations of the facet surfaces, resulting in slope error distributions across the reflective surfaces. The geometry of the LUZ LS-2 parabolic trough collector was modeled in SolidWorks, and the effects of gravity on the reflective surfaces are analyzed using SolidWorks Simulation. The ideal mirror shape, along with the 90° and 0° positions (with gravity deformation) were evaluated for the LS-2. The ray-tracing programs APEX and ASAP are used to assess the impact of gravity deformations on optical performance. A comprehensive study is performed for the parabolic trough to evaluate a random slope error threshold (i.e., induced by manufacturing errors and assembly processes) above which additional slope errors caused by gravity sag decrease the intercept factor of the system. The optical performance of the deformed shape of the collector (in both positions) is analyzed by first modeling the ideal collector without deformation. This provides the study with a control since the optical performance is as good as possible for the undeformed model. Next, the deformed collector model is analyzed in the ray trace. Finally, additional induced slope errors ranging from zero up to 1° (17.44 mrad) are applied to the solar collector surface (undeformed and deformed models) to evaluate the degradation in optical performance. The ray trace results for the

deformed models are compared to the undeformed model to evaluate when induced slope errors due to gravity loading impact optical performance for each collector orientation. This is further referred to as a threshold approach. Another ray trace analysis can be used to identify the intercept factor for different solar incident angles. The intercept factors are found from ray-tracing and then compared to empirical data to demonstrate if the simulations provide consistent answers with experimental data.

5.2.3   Ray Trace Analysis Setup

The FEA produced deformed geometry, which could then be saved and imported into a ray-tracing model as shown in Figure 19. A ray trace model needs three essential objects for solar collecting systems. The first is the emitting source which is the sun for solar applications. The second is the actual collecting system. The structure for the reflecting surfaces does not need to be included if it does not interfere with the reflection of solar radiation to a target. The third object is the target. The target is where rays are terminated (fully absorbed if they reach the target) and this object is where ray trace optical performance statistics are commonly extracted from. For a parabolic trough the target is the HCE which is composed of the glass envelope and absorbing element. In general, a ray trace procedure acts as follows:

1) The rays are emitted into the model from the emitting source.

2) The rays travel in their respective directions until they are either reflected, transmitted, or absorbed by the objects in the system.

   a) If absorbed then the ray is terminated on the absorbing object.

   b) If reflected, the ray continues in the ray trace until it is absorbed.

c) If transmitted, the ray continues to be traced in the system until it is reflected or absorbed.

3) The ray trace is complete when all of the rays in the system are terminated. A ray is either terminated when it is absorbing by an object in the system or if it leaves the system as a "missed" ray meaning it failed to be absorbed by any object.

For solar models, a custom "sun" object has to be created within each ray-tracing program above the solar collector. In ASAP, a rectangular object was created and then set to emit rays. The rays were set to have a half-angle emission from the sun source of 4.8 mrad (0.275°) with the sun apodization applied over that half-angle. This setting properly applies the sun limb-darkening (apodization) to the model. The sun source is easily modified to not include the apodization effect by simply removing it from the program script. In APEX, a similar rectangular object is created and set to emit rays. The rays are emitted normal from a surface and then pass through a Lambertian "scatter model" which forces the rays to be emitted with the same cone angle as the ASAP case, shown in Figure 17. A Lambertian model scatters rays in every direction with the same magnitude. When applied with the sun cone angle this approximates the sun most appropriately when limb-darkening is not included. This sun-source does not have the ability to be apodized to resemble the true sun cone-angle intensity. A sensitivity study in ASAP was run to evaluate the effect of not including limb-darkening. The comparison showed that the absolute intercept factor was reduced by one percentage point leading to the conclusion that the APEX sun model would be a valid tool to show that the modeling methodology presented here can be used to achieve fairly accurate results.
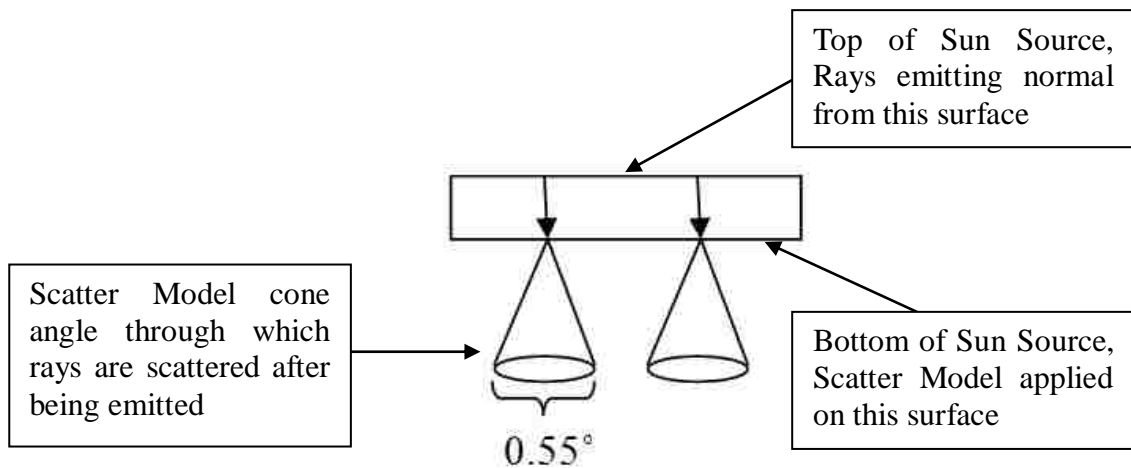
Figure 17. Sectional view of APEX emitting sun source, rays being emitted from top surface, then scattered randomly into the 0.55° cone angle

The ray-trace simulations used a deterministic modeling approach meaning that the same results are achieved for every ray trace when identical parameters are used. A Monte Carlo method is available in APEX, but was not feasible for this study due to the modeling approach taken to simulate a sun source. The APEX scatter model is a Lambertian model limited by a small scatter cone angle of ~0.55° which limits the transmission of rays through the surface unless a very large number of rays are traced. There is a small probability that the rays are scattered through the surface in the small cone angle required by the sun model resulting in most of the rays being absorbed by the scattering surface. This is an artifact of using the Lambertian surface and how the internal Monte Carlo algorithm works. APEX help states that for deterministic modeling, the number of scattered rays need only be one if the scattering angle is less than 5.7°. This particular model is deemed to be accurate since the number of scattered rays is set to ten and the cone angle is only ~0.55°.

The sun emitting source was made to move to its estimated position in the sky according to the day of the year, latitude, and the hour relative to solar noon [18]. The parabolic trough is aligned longitudinally along the north-south axis (+Z direction is north, +X is west) and made to track the sun. The sun's azimuth angle is negative when in the east and positive when in the west. The sun's elevation angle is always positive with 90° being the sun directly overhead.
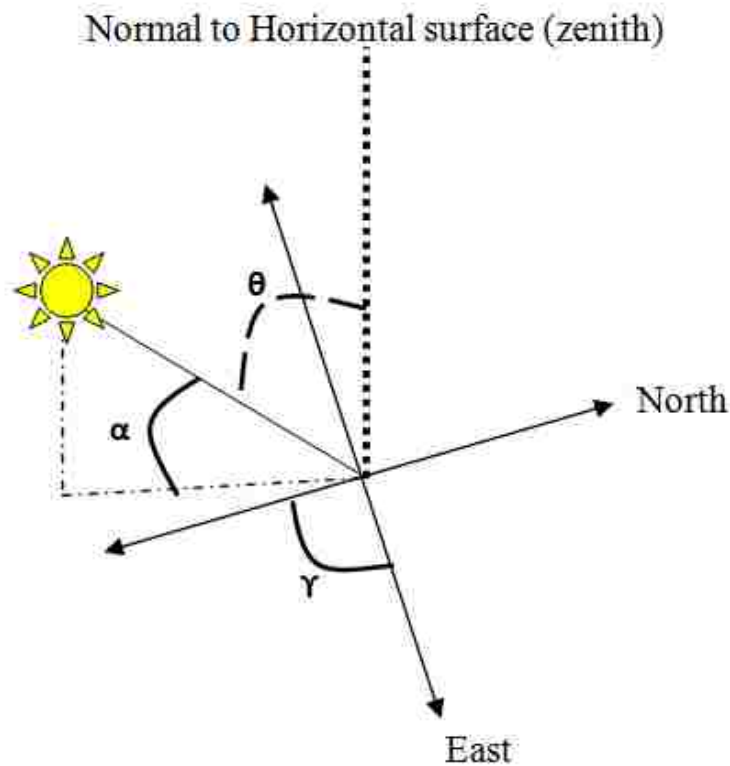
Figure 18. Sun direction schematic, α is the elevation angle, ϒ is the azimuth angle, and θ is the incident angle

In both APEX and ASAP, specific boundary conditions (surface coatings, part material) needed to be applied to each surface of the imported FEA geometry to achieve an accurate ray-trace of each model.

An emitting surface is applied to the top of the sun object (rectangular volume in APEX) with 1 million rays emitted towards the collector with a prescribed direct normal irradiance (DNI) of 1000 W/m^2 with a constant ray wavelength of 550 nm. The sun source initially emits 100,000 rays which pass through the sun scattering surface (bottom of sun object) causing the rays to scatter within the sun cone angle specified. Each ray is split into 10 rays that pass onto the rest of the model from the scattering surface. Each of those ten rays are restricted to the Lambertian scatter model such that each ray has the same magnitude independent of the direction it is scattered within the sun cone angle.

Also applied to the sun source, is a simple coating designed to kill the parent rays and only allow their children rays to pass on to the rest of the model. The reason for killing the parent ray is to generate a reasonable distribution of rays upon the trough from the scattering surface without the influence of the initial parent rays. This better represents a sun source by forcing the parent ray to be distributed into the sun cone angle. The medium of the sun source was set to "air" to allow the rays to pass with near 100% transmissivity through the simulated source. The sun source size is arbitrary as long as it is sufficiently large to generate enough rays to strike all parts of the model.

The parabolic trough HCE is made to extend well past the collector in both the north and south directions to make sure that there are no end losses in this model. It is located at a focal length of 1.49 m from the collector. The HCE tube is composed of two components, the outer glass envelope and the absorbing element. The outer envelope is made of Schott N-BK7 glass medium with refractive index of 1.5168 which is a borosilicate type glass. The medium allows for ray distortion as they pass through the envelope. Total internal reflection is also possible and, if a ray encounters this

phenomenon, it will eventually terminate within the glass envelope counting as a missed ray. The outer diameter of the glass envelope is 115 mm and has a thickness of 3 mm. Additional anti-reflective (AR) coatings were applied to the outer and inner surfaces of the envelope which had 3% reflectivity and 97% transmissivity based upon Sol-Gel AR coating experimental values [19]. It should be noted that these values are not precisely known for the actual parabolic trough tube. The anti-reflecting coating does not have an explicit thickness applied because it is assumed that the coating strictly behaves as a single layer of quarter-wave coating. The 3% absorption value is dependent on the incoming incident angle of the solar rays. Higher incident angles have more reflection than transmission. However, the AR coating is supposed to help reduce absorption with increasing incident angle. The transmissivity coefficients are directly dependent on the incident angle of the incoming rays and the refractive index of the media. The ray wavelength is constant throughout the study. Anti-reflective coatings are designed based on the concept of dielectric reflection which is explained explicitly by Stine and Harrigan [2]. The absorbing element is made to be perfectly absorbing with a diameter of 70 mm. 100% absorptive causes all rays to terminate at the HCE. This gives accurate intercept factor results when considering only the number of rays hitting the HCE. However, any heat transfer results in the system would be skewed due to reflection losses not being accounted for. This parabolic trough tube simulates the Schott PTR-70 receiver model except for the perfect absorption.

The collector geometry for the ray trace is composed of the four mirror surfaces of the LS-2 since the truss system does not impact the ray-trace analysis. The non-relevant parts in the ray trace were suppressed from the deformed model. The mirrors are

set to be perfectly reflecting for this analysis to compare the performance characteristics of the trough mirrors for each model. If wanted, the mirrors can also be set to absorb a certain amount of the incoming radiation, but this fraction would be small. This condition is used in conjunction with surface roughness models to simulate ray scattering when reflected from the mirror surfaces. The roughness models act as an additional RMS slope error on the mirror surfaces caused by manufacturing defects or cleanliness. The roughness models are added to the models in increments to evaluate at which point gravity induced slope errors contribute to degradation in optical performance. These coatings are custom created scatter models which are utilized to simulate a roughened surface. However, due to a current APEX bug, it is not possible to set the slope error to exactly 5 mrad or 10 mrad. Due to the number of significant values acceptable, a slope error of 5.23 mrad (0.3°), 10.47 mrad (0.6°), and 17.44 mrad (1°) are chosen for each custom roughness coating value. Ray trace studies not previously mentioned were performed by adding additional lower RMS slope error values to the mirror surfaces. These values were similar to the slope error results observed by Ulmer [5] of about ~4 mrad. The initial results showed that gravity induced slope errors in these cases did not contribute significantly to decreased intercept factors between the ideal and deformed models. Therefore, a simulation scheme using higher RMS slope error values was established to try and determine if there was an error threshold above which additional gravity induced slope errors would impact the intercept factor significantly. The decreased intercept factor threshold can be directly determined by comparing the ideally shaped model intercept factors to the gravity deformed trough model results. If the intercept factors differ between the ideal and deformed models then it is a result due to

the gravity-induced slope errors in the deformed system. Although unrealistic, using the higher RMS slope error values gives a good range of comparison for the ray-trace models.
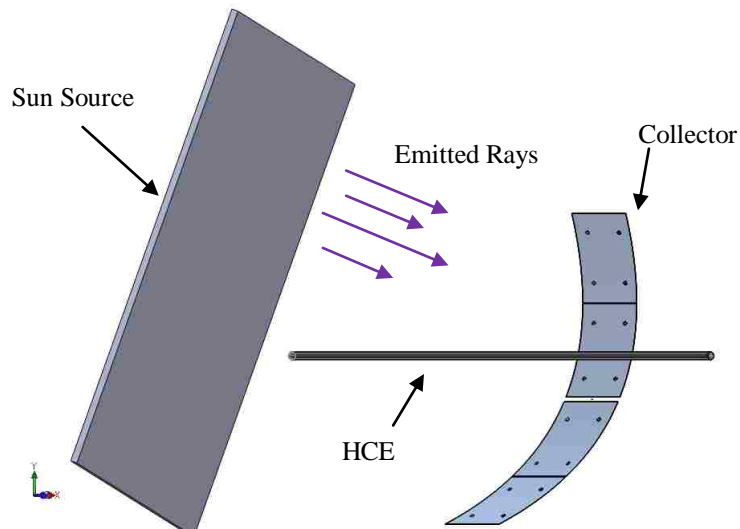
Figure 19. Ray-Tracing model; sun-source, HCE with envelope, and collector

5.2.4   Ray Trace Analysis

5.2.4..1   Intercept Factor Threshold Analysis

The optical performance of the parabolic trough is quantified using the intercept factor of the system. The intercept factor was calculated as shown in Equation 1. This equation provides a calculation of the intercept factor for the system including all possible rays which missed the HCE.   Although the equation is simplified here, the numerator consists of the several objects in the model for which the ray trace results can be extracted from. These objects are the HCE components and the collector.

$$\mathbf{I.\,F.} = \frac{\textbf{Power from the collector hitting the receiver}}{\textbf{Total power reflected from the collector}} \; ; \qquad (1)$$

where I.F. is the intercept factor.

In the ray-tracing models there are inherent difficulties in obtaining an accurate intercept factor. When the sun emits rays, some of the rays hit the HCE directly without touching the collector. This provides inaccurate results because the intercept factor should only include the rays that reflect from the collector and strike the absorbing element. Therefore, the rays hitting the HCE directly were subtracted from the intercept factor calculation. These rays are found by setting the collector reflecting surfaces to a perfectly absorbing material and then running the ray trace. At this point, any rays that strike the HCE are directly from the sun and this number can be subtracted from further ray trace studies when rays are being reflected to the HCE from the collector.

To determine if gravity-induced deflections have a significant impact on intercept factors, a ray trace study was done which compares three collector models: ideal shaped mirrors (undeformed model), 0° position deformed mirrors, and 90° position deformed mirrors. Each trough model had four cases evaluating different additional roughness values on the collector reflective surfaces for two different incident angles. The roughness cases include additional slope errors on the mirrors of 0 mrad, 5.23 mrad, 10.47 mrad, and 17.44 mrad. In total, there are 24 cases being evaluated.

Each model was also evaluated in two positions while tracking the sun at solar incident angles of 44.22° (9am) and 58.32° (solar noon) on December 21 (day 355 of an average year). The latitude for the model used was for Daggett, CA (34.867°N). Figure 20 displays the ray-trace for the 44.22° sun incident angle while viewing perpendicular to the north-south axis. These incident angles were chosen arbitrarily, but are thought to give a good comparison for the impacts on intercept factors when the incident angles vary

significantly. In addition to modeling the worst-case deformation positions, these angles provide a clear comparison of the effects of gravity deformations on trough optical performance when the sun is not normal to the surface.

In summary, each model was evaluated with eight ray-tracing scenarios (4 for each incident angle) in order to evaluate a random slope error threshold (i.e., induced by manufacturing errors, assembly processes, or cleanliness) above which additional slope errors caused by gravity sag decrease the intercept factor of the system. Figure 21 displays some representative ray-trace figures of HCE ray intercepts. This particular case is for the ideal shaped mirrors with 0, 5.23, 10.47, and 17.44 mrad applied at an incident angle of 58.32°. Most of the ray-trace figures look visually similar. Figure 22 and Figure 23 display a typical view of the parabolic trough with sun incident angles of 58.32° and 44.22°, respectively. Note the difference in distance that the rays travel from the collector to the HCE with increasing incident angle in the figures. Some of the rays are striking the tube directly from the sun source and these appear as hitting the top of the tube in the figure. These rays are subtracted from the final intercept factor values since they do not contribute to the intercept factor considering only the reflected rays from the collector to the HCE. It can be visually verified from this figure that there are no end losses considered in any of the cases.

Several ray-traces were performed in ASAP mimicking the optical properties set in APEX. This analysis found that APEX was performing the ray-tracing accurately. When compared, the results from each program were near identical.
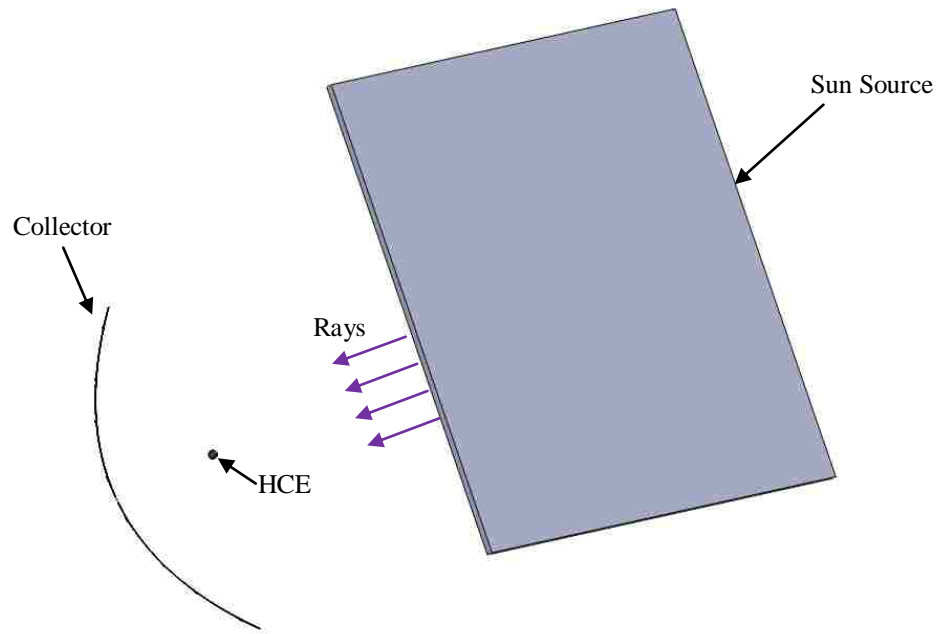
**Figure 20. Perpendicular to North-South axis view of LS-2 trough at a 44.22°
incident angle on Day 355**
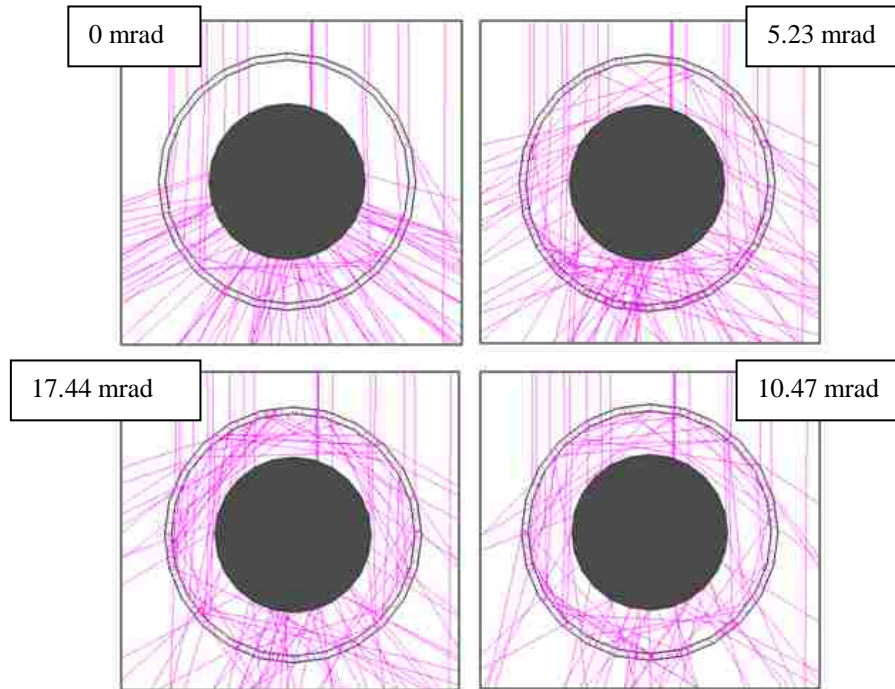
Figure 21. 58.32° incident angle HCE intercept figures for the undeformed trough, (From top-left clockwise) 0 mrad, 5.23 mrad RMS, 10.47 mrad RMS, and 17.44 mrad RMS applied; any rays not hitting the HCE are terminated on the last contacted surface; vertical lines coming from the top of each figure are rays directly from the sun; every 1000 of 1 million rays displayed
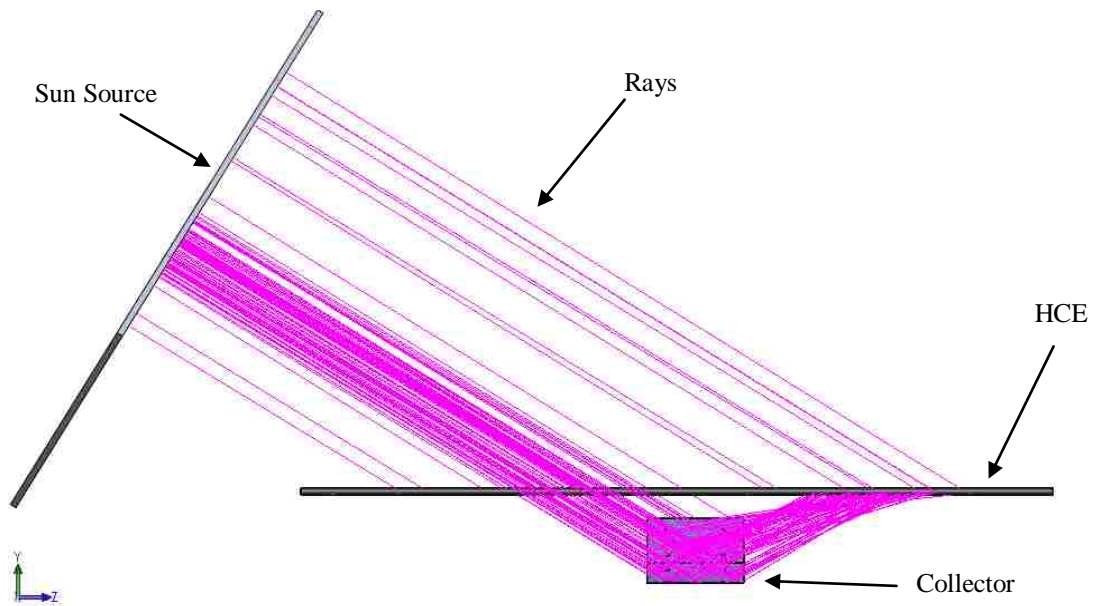
Figure 22. 58.32° incident angle ray-trace model for ideal shaped mirrors, tracing every 1000 ray; viewing west
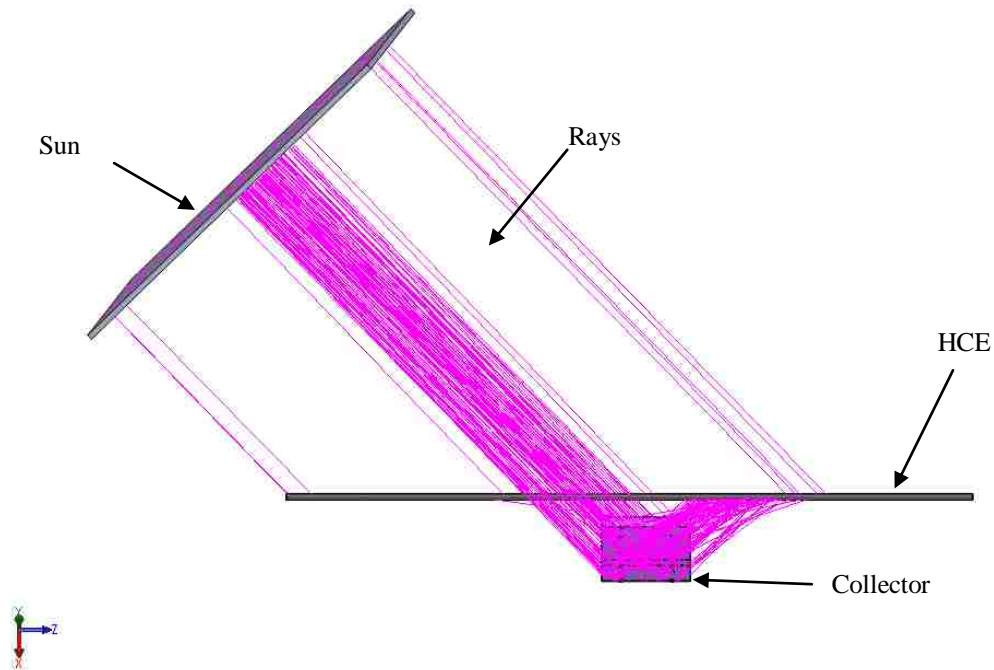
Figure 23. 44.22° incident angle ray-trace model for ideal shaped mirrors, tracing every 1000 ray; rotated west view to visualize ray path

Figure 24 and Figure 25 show the decreasing trends in intercept factors when additional slope errors are added to the reflective surfaces. The trends are nearly identical

Table 4 and Table 5 display the intercept factor percent differences of the 0° and 90° positioned deformed models when compared to the ideally shaped mirrors at solar incident angles of 44.22° and 58.32°. As the additional slope errors are applied to the mirror surfaces, the intercept factor percent differences between the ideal and deformed models are less than 1% and in most cases less than 0.5% leading to the conclusion that gravity-induced deflections in the mirrors are not significantly impacting the intercept factors of the LS-2 collector based on the FEA performed on this particular trough model. The ideal mirror intercept factors are close to the deformed model intercept factors. A threshold was not reached where gravity-induce slope errors caused the deformed model's intercept factors to deviate significantly from the ideal case.

Figure 24. Intercept factors with increasing additional slope errors present on the reflective surfaces for the incident angle of 44.22˚ for the deformed models and ideal model

Figure 25. Intercept factors with increasing additional slope errors present on the reflective surfaces for the incident angle of 58.32˚ for the deformed models and ideal model

Table 4. Intercept factor percent differences for Ideal vs. 0° deformed model

	Solar incident angle: 44.22°	Solar incident angle: 58.32°
No additional slope errors	0.04%	0.07%
5.23 mrad RMS additional slope error	0.06%	0.09%
10.47 mrad RMS additional slope error	0.32%	0.64%
17.44 mrad RMS additional slope error	0.07%	0.70%

Table 5. Intercept factor percent differences for Ideal vs. 90° deformed model

	Solar incident angle: 44.22°	Solar incident angle: 58.32°
No additional slope errors	0.08%	0.05%
5.23 mrad RMS additional slope error	0.17%	0.10%
10.47 mrad RMS additional slope error	0.13%	0.03%
17.44 mrad RMS additional slope error	0.28%	0.04%

Some of the trends are counter intuitive for the percent differences between the deformed models and ideal model at different solar incident angles. The rays have a shorter distance to travel from the mirrors to the HCE as the solar incident angle increases, as can be verified from Figure 22 and Figure 23. In geometric terms, the rays reflect off the mirror surfaces (influenced by gravity induced slope errors and additional roughened surface slope errors) at a certain angle. Depending on the solar incident angle, the distance the rays travel from the reflective surfaces to the HCE can be significant. Rays reflected with significantly distorted angles can miss the HCE completely

depending on the distance they have to travel before they hit the HCE. The 0° model was influenced by the longer ray travel distance. At a solar incident angle of 44.22°, the slope errors do not impact the reflected ray angles enough to cause the rays to miss the HCE. However, at a solar incident angle of 58.32°, the reflected ray angles cause more rays to miss the HCE due to the longer travel distance.

The trend is opposite for the 90° position case. At a solar incident angle of 44.22°, the intercept factor differences are higher than at a solar incident angle of 58.32°. Some of the reflected rays do not impact the HCE with a shorter distance to travel. However, the longer distance allows the reflected ray angles to strike the HCE. The longer distance aids the reflected rays in a positive way. It is reasoned that the gravity displacements in the 90° deformed model actually aid in increasing the intercept factor.

These effects are still mitigated by the fact that the intercept factors are not significantly impacted by deformations when compared to the ideal shaped mirror as can be seen by the very low percent differences.

5.2.4..2   Intercept Factor Incident Angle Dependence

Experimental intercept factor studies were performed on the LS-2 trough by Dudley et al. [1] which lend a valid comparison to the ray-trace studies. The performance degradation of the trough was evaluated as the solar beam incident angle changed. Dudley utilizes thermal measurements to determine the intercept factors of the HCE based on solar incident angle. In the study, cold water is used as the heat-transfer fluid and operation is at ambient air temperatures leading to low thermal losses. Although the true optical efficiency can only be measured if thermal losses were zero, this approach provides a good approximation for the trough intercept factors since the operating system

was kept as close to ambient temperature as possible. The ray-trace analysis provides a way to estimate the RMS slope error on the experimental collector mirrors by comparing the simulated and empirical results. However, the ray-trace does not include any losses from the HCE which could cause minor differences between the experimental and simulated results.

The experimental studies resulted in Figure 26, detailing the calculated intercept factor of the system. The calculation required to achieve a comparable intercept factor to the ray-trace results is seen in Equation 2.

$$\text{I. F.}'_{\text{Data}} = \frac{\textbf{Incident Angle Modifier}}{\textbf{cos(solar beam incident angle)}} \; ; \tag{2}$$

where I.F.$'_{\text{Data}}$ is the normalized intercept factor relative to the intercept factor at a zero incident angle for the empirical results. The incident angle modifier (K) is found from substituting the solar beam incident angle into the respective equations shown in Figure 26.

Since the gravity-induced deflections in the model were discovered to not severely impact intercept factors for the deformed FEA model in this analysis, only the ideal shaped trough model was used for comparison to the experimental results. Four days were evaluated at solar incident angles relative to solar noon. The days were March 21 (day 80), June 21 (day 172), September 23 (day 266), and December 21 (day 355) which correspond to solar incident angles of 35.27°, 11.43°, 35.88°, 58.32°, respectively. March 21 and September 23 has close to the same incident angles, but this is to show that close incident angles perform in a similar way as a check for the ray trace simulation. If the

intercept factors for the close incident angles don't perform as expected then this gives clear reason that something is not correct in the simulations. The days chosen were the equinoxes and solstices. The three cases for the ideal model were additional RMS slope errors of 0 mrad, 5.23 mrad, and 10.47 mrad applied to the reflective surfaces. It is assumed in the ray-trace simulations that the HCE is ideally located, however in reality the HCE sags when in different orientations. However, as a first estimate, the comparison of simulation results to experimental results should still be fairly close and a more detailed FEA could be applied to account for this sagging effect in future studies.

In the ray-trace, the intercept factor for a particular incident angle needs to be modified in order to compare to the empirical data intercept factor, shown in Equation 3.

$$\mathbf{I.F.'_{ray\_trace}} = \frac{\mathbf{I.F.\ of\ incident\ angle}}{\mathbf{I.F.\ of\ zero\ incident\ angle}}\ ; \tag{3}$$

where I.F.$'_{ray\_trace}$ is the normalized intercept factor relative to the intercept factor at a zero incident angle for the ray-trace results.

Figure 29 and Figure 30 show the cross-sectional view of the HCE with rays striking the HCE reflecting from the collector with increasing solar incident angles. The number of rays striking the HCE decrease with increasing solar incident angle. It should be noted that the error bars result from an error analysis performed for this study. It is determined that the error is +/- 1.88% for the incident angle modifier in the experimental data [1].
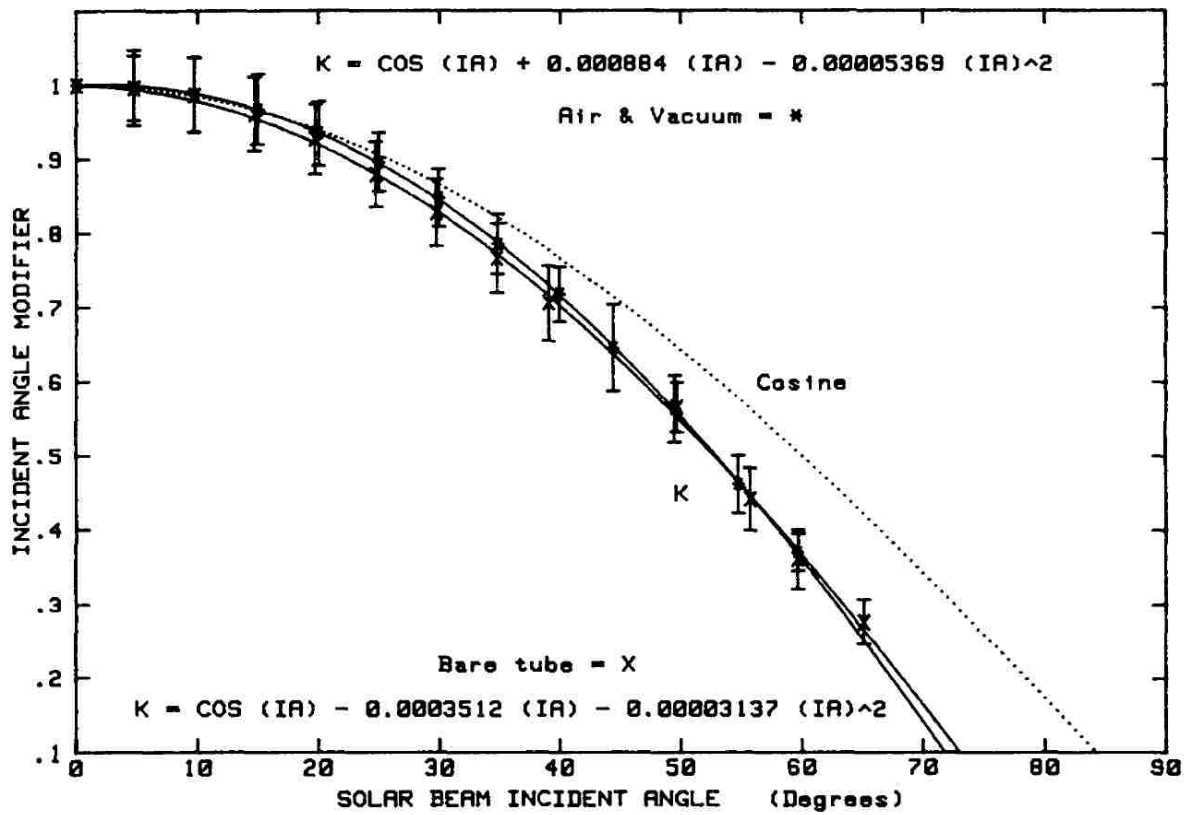
Figure 26. Incident angle modifier for LS-2 receiver [1]

Figure 27 and Figure 28 show the ray-trace simulations for solar incident angles of 35.27° and 11.43°, respectively.

Sun Source

Rays

HCE

Collector
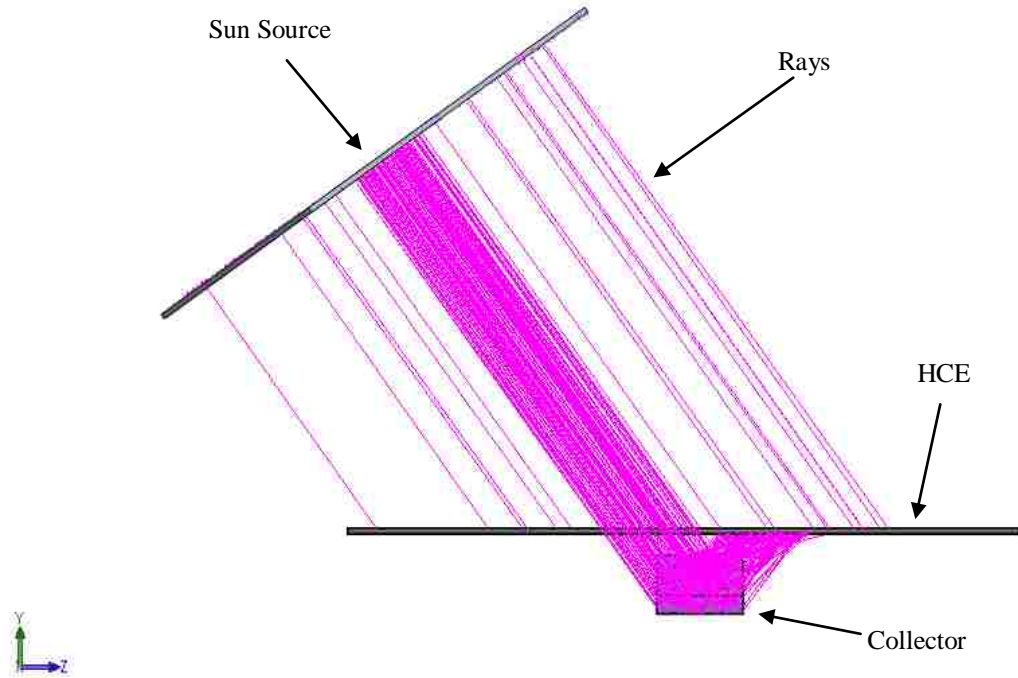
Figure 27. Day 80 (Spring Equinox) ray-trace simulation for comparison to empirical data

Sun Source

Rays

HCE

Collector
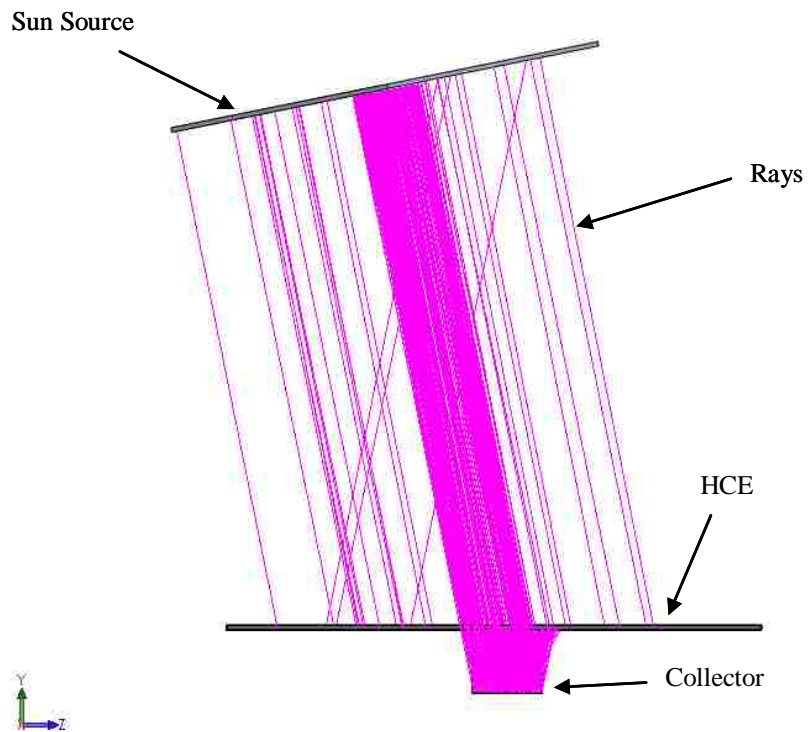
Figure 28. Day 172 (Summer Solstice) ray-trace simulation for comparison to empirical data
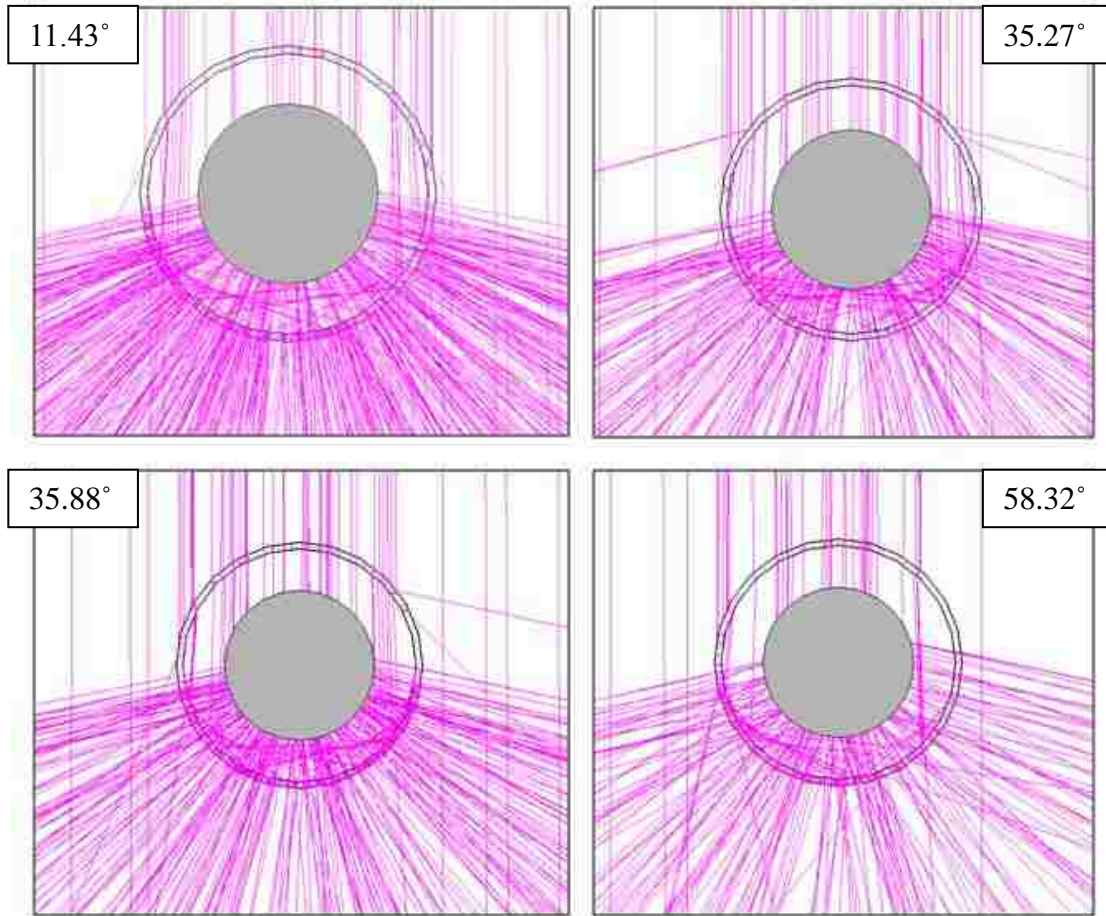
Figure 29. Increasing incident angle and the influence on HCE intercept figures for the undeformed trough with 0 mrad additional RMS slope errors applied to reflective surfaces, (From top-left clockwise) 11.43°, 35.27°, 58.32°, and 35.88; any rays not hitting the HCE are terminated on the last contacted surface; vertical lines coming from the top of each figure are rays directly from the sun; every 1000 of 1 million rays displayed
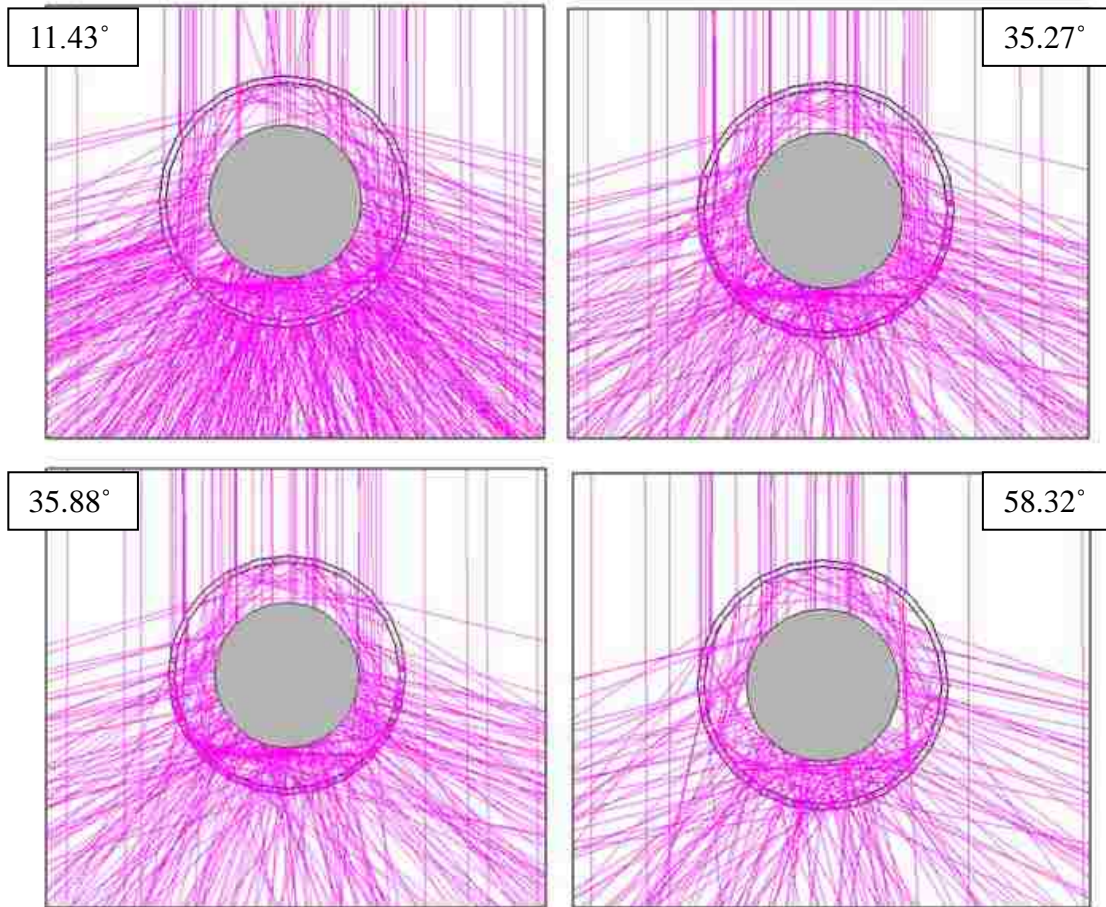
Figure 30. Increasing incident angle and the influence on HCE intercept figures for the undeformed trough with 5.23 mrad additional RMS slope errors applied to reflective surfaces, (From top-left clockwise) 11.43˚, 35.27˚, 58.32˚, and 35.88; any rays not hitting the HCE are terminated on the last contacted surface; vertical lines coming from the top of each figure are rays directly from the sun; every 1000 of 1 million rays displayed

The ray-trace simulation results are presented in Table 6, Table 7, and Table 8. These three tables compare the ray-trace intercept factors with the empirical data intercept factors at the different solar incident angles (θ). A negative percent difference indicates that the ray-trace intercept factor is below the empirical data result. A positive value means the ray-trace intercept factor was estimated above the empirical data result.

Table 6. Ideal LS-2 shape intercept factor with empirical data percent difference

Θ (°)	Empirical Intercept Factor	Ray-Trace Intercept Factor	Percent Difference
35.27	0.968	0.930	-3.96%
11.43	0.990	0.937	-5.50%
35.88	0.963	0.930	-3.48%
58.32	0.762	0.860	12.12%

Table 7. Ideal LS-2 shape with 5.23 mrad additional RMS slope error intercept factor with empirical data percent difference

Θ (°)	Empirical Intercept Factor	Ray-Trace Intercept Factor	Percent Difference
35.27	0.968	0.913	-5.82%
11.43	0.990	0.934	-5.78%
35.88	0.963	0.911	-5.49%
58.32	0.762	0.791	3.74%

Table 8. Ideal LS-2 shape with 10.47 mrad additional RMS slope error intercept factor with empirical data percent difference

Θ (°)	Empirical Intercept Factor	Ray-Trace Intercept Factor	Percent Difference
35.27	0.968	0.870	-10.67%
11.43	0.990	0.901	-9.32%
35.88	0.963	0.867	-10.44%
58.32	0.762	0.728	-4.59%

It is clearly seen that the intercept factors differ significantly from the simulations and empirical results. This gives reason that the single trough mirror column cannot accurately be used as an optical performance indicator for an entire trough module. The full trough module would need to be modeled which is described in Section 6.2 of this report.

Another reason for the large percent differences in intercept factors for the empirical data and ray-trace results is likely caused by unknown reflectivity values for the experimental LS-2 glass envelope. It was known that an anti-reflective (AR) coating was applied to the glass envelope, most likely Sol-Gel coating, but the reflectivity was assumed to be 3%. This value was most likely lower in the experimental setup causing the intercept factor for the trough to be higher in the empirical data. Dudley et al. [1] performed a study evaluating the impact of the glass envelope on the intercept factors. They found that removing the glass envelope did not have an impact on the trough intercept factor. This supports the conclusion that the values reported by Pettit et al. [10] were higher than the value of the AR coating on the experimental glass envelope. A few simulations were run with a perfectly transmitting glass envelope and 0 mrad additional slope errors on the ideal LS-2 model. This led to intercept factors as high as 0.99 for the ideal case. This shows the reflectivity of the envelope is critical in predicting the intercept factors of the system along with finding an accurate representation of the additional RMS slope errors due to defects and cleanliness.

5.2.5 Ray Trace Analysis Conclusions

A procedure is developed to evaluate the optical properties of solar collector systems. Ray-trace simulations were performed on the LS-2 parabolic trough utilizing FEA results. A comprehensive analysis was performed for the parabolic trough to evaluate a random slope error threshold above which gravity-induced deflections decrease the optical performance of the trough system. The intercept factor for an ideal mirror shape and deformed shapes due to gravity in the 0° position and 90° position were found using ray-trace measurements. These positions were chosen based on the assumption that they

provide the greatest deformed trough surfaces. The deformed models were used as inputs in a ray trace. The ray trace simulations were composed of different emitting solar incident angles and varying additional RMS slope error values applied to the reflective surfaces. As the additional errors are applied to the deformed models, it is reasoned that when compared to an ideal model with the same additional errors applied, any difference in intercept factor will be attributed to gravity-induced deformations. Thus, a threshold approach is created to evaluate the effects of gravity deformation on trough optical performance.

The 0° positioned deformed model resulted in the highest percent differences when compared to the ideal shaped mirrors of ~0.3% at a solar incident angle of 44.22° and ~0.7% at 58.32°. The 90° positioned trough intercept factor differences were slightly lower than the 0° case. This result shows that the single mirror column's optical performance is not affected by gravity induced displacements in the mirrors. If the single mirror column were a whole collector system, then this system is designed structural sound so that gravity does not impact the optical performance. However, the single mirror column was used as a procedural example of how FEA and ray tracing can be combined to evaluate the optical performance of a collector. The conclusion that gravity does not impact the optical performance of a single mirror column may not be the case for the full size trough module. The full size trough module is evaluated in Section 6.2 of this report.

A performance degradation study of the LS-2 system was evaluated for varying solar incident angles. Empirical data was compared to ray-tracing results to evaluate the plausible additional RMS slope error present on the experimental LS-2 trough at the

NSTTF. The intercept factors for the empirical and ray-trace results differed significantly leading to the conclusion that a single trough mirror column can not accurately be used as an optical performance indicator for a full trough module. Another difference for large intercept factor differences is most likely attributed to a higher AR value being applied to the glass envelope in the ray-trace simulations. However, with further work to evaluate the true reflectivity value of the glass envelope surrounding the HCE and using more realistic additional RMS slope errors on the simulated mirrors, a better ray-trace result can be achieved and compared directly to the experimental results.

6. OTHER ANALYSES

6.1 Further Use of Slope Error Analysis

SkyFuel, a parabolic trough company, requested the slope error procedure be performed on one of their parabolic trough designs. According to www.skyfuel.com, "The SkyTrough is SkyFuel's high-performance parabolic trough solar concentrator for use in utility-grade solar-thermal power plants for generating electricity or for industrial process heat applications" [20]. This trough differs from other designs because it utilizes a unique reflective mirror surface called ReflecTech Mirror Film. The mirror film is applied to an aluminum sheet that acts like traditional parabolic trough mirror structures. The slope error analysis was performed and the results were given to SkyFuel so they could evaluate their system design. Unfortunately, explicit detail cannot be provided here due to proprietary issues. The ray-trace portion of this analysis was not yet fully developed during the SkyFuel analysis so it was not applied to this system.

6.2   Full LS-2 Parabolic Trough Module

Although the single mirror columns of the LS-2 trough are independent of each other, the effect of a displacing torque tube may further affect the trough displacements due to gravity. The sag of the HCE will also be simulated in order to allow for a more accurate comparison between the numerical and empirical results. As a result, the optical performance will be compared to experimental results presented by Dudley [1].

6.2.1   FEA Displacements

The full parabolic trough was subjected to gravity loading in the 0° and 90° positions. The mesh for the FEA has the same settings as for the single mirror column except for an extra mesh control to account for the glass envelope on the HCE. An element size of 0.8391 in was applied to this part. The full trough had 1,203,269 elements. A grid convergence study was performed to make sure this mesh provided accurate and consistent displacement results. The boundary conditions for the FEA are shown in Figure 31. The green arrows note the fixed boundary condition while the red arrow indicates the gravity loading vector.
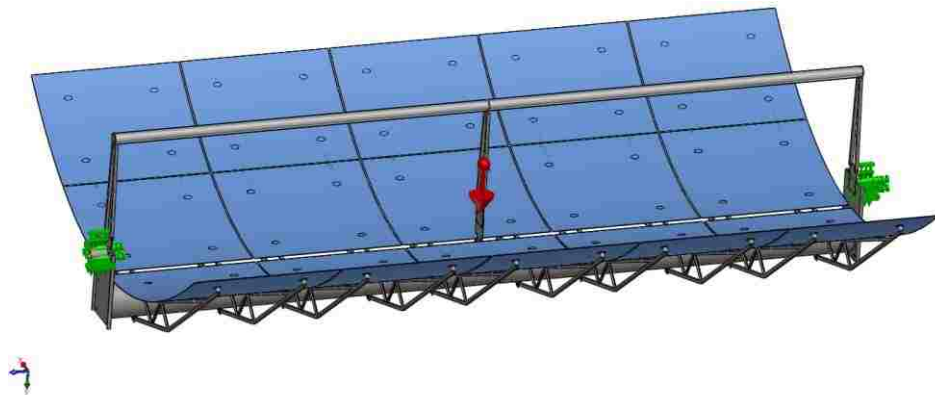
Figure 31. 90° position full LS-2 parabolic trough module with FEA restraints and loading. Red arrow indicates gravity loading. Green arrows indicate fixed restraints.

After running preliminary analysis, it was determined that the 90˚ position provided the most interesting results in terms of gravity induced slope errors. This position degraded the optical performance of the system more than the ideal parabolic shape collector. An initial ray trace was performed on the deformed and ideal models to see if there were differences in the optical performances of the system when additional slope errors were added to the reflective surfaces. This particular ray trace used a solar incident angle of 35.27˚. The HCE glass envelope was excluded from the full trough model because the specifications of the glass envelope are not precisely known and were shown to significantly impact the intercept factor of the system described in Section 5. However, the empirical results provide values for optical performance without the glass envelope so there is still valid empirical data to compare the numerical data to. Table 9 shows the same threshold approach as described in Section 5, but for the full trough module. The 0˚ positioned deformed model and the 90˚ positioned deformed model were compared to the ideal shaped parabolic trough with 0 mrad, 5 mrad, and 10 mrad of additional slope errors applied to the reflective surfaces of the models. The results show that the ideal and 90˚ deformed models differ significantly in terms of intercept factors. The 0˚ deformed model differed slightly from the ideal shape. These are significant results since the single trough module described in Section 5 showed that gravity induced deformations did not contribute to the degradation of optical performance in a single mirror column. The results presented here show that in the full trough system gravity sag plays an important role in the optical performance of the system.

Table 9: Intercept factors for Ideal and Deformed parabolic trough models with additional slope errors applied to the reflective surfaces, Solar incident angle of 35.27˚

	Ideal Shape of Parabolic Trough Intercept Factor	90˚ Deformed Trough Intercept Factor	0˚ Deformed Trough Intercept Factor
0 mrad	0.996	0.996	0.996
5 mrad	0.919	0.769	0.901
10 mrad	0.686	0.582	0.669

The preliminary ray trace showed that the most interesting position for trough deformation and optical degradation is in the 90˚ position. Thus, from this point forward in the analysis only the 90˚ position will be analyzed. Another reason that this deformed model is being considered over the 0˚ position for the full ray trace analysis is that during the empirical testing, it is known that the trough was positioned facing the sun during the most sunny times during the day for testing. The test dates for incident angle tests were roughly August through September which correspond to sun elevation angles of 73˚-51.3˚(days 213-273 respectively). These elevation angles correspond to the trough being positioned facing more upward toward the sky rather than towards the horizontal which the 90˚ position represents. It is reasoned that the deformations incurred at the 90˚ position would be the worst gravity induced deformations in the system thus provide a worst-case scenario analysis, but still can be roughly compared to the empirical results for model validation purposes.

The 90˚ position displacement plots from SolidWorks Simulation are shown in Figure 32, Figure 33, and Figure 34. It can be seen that the trough displacements are quarter-symmetric about the torque tube axis and down the center of the middle mirror column axis. The displacements indicate an opening clam-shell effect where the mirror columns displace outward away from the torque tube causing the mirror columns to

"open up". Figure 35 shows the displacements in the trusses and torque tubes for the full

size model. They are relatively lower than those present in the mirrors.
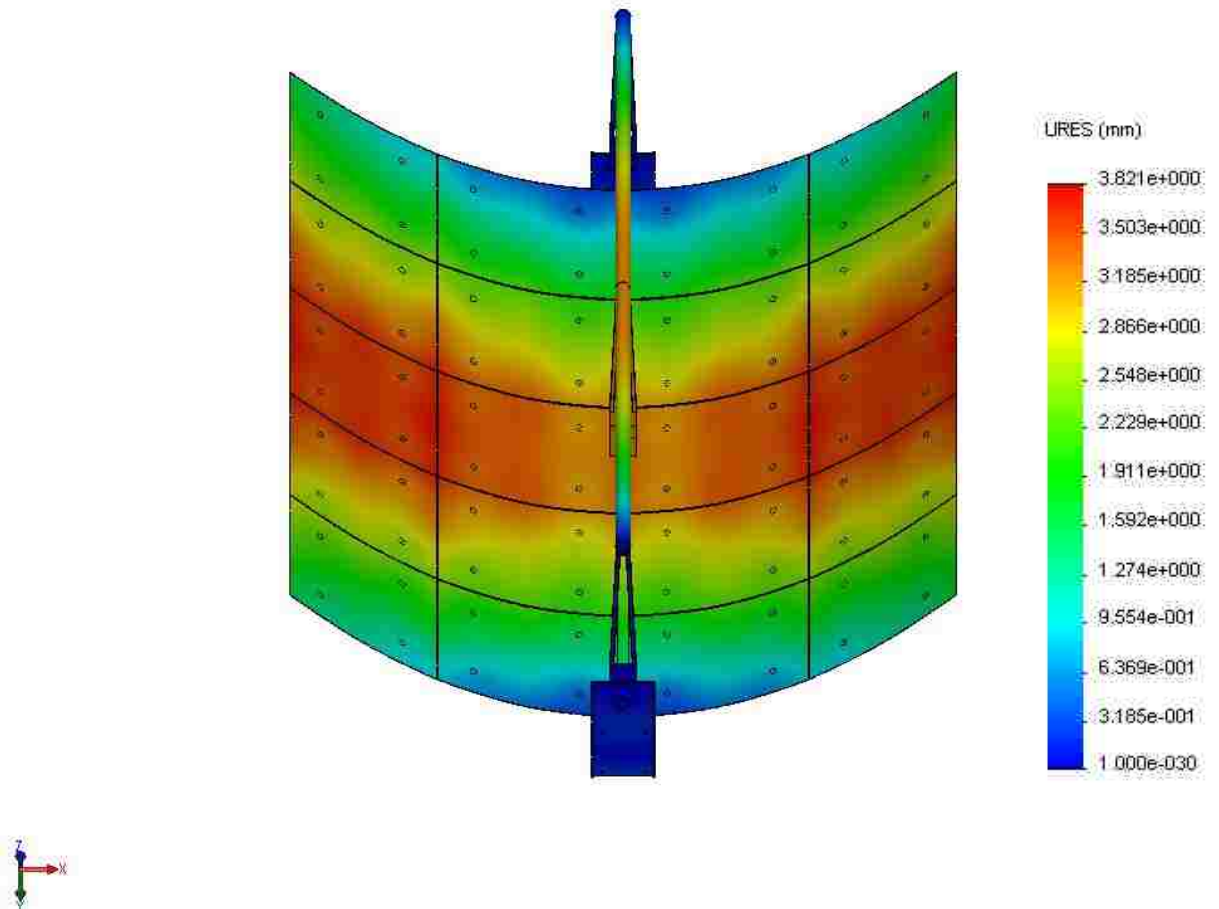
Figure 32: 90° deformed parabolic trough looking lengthwise along the collector, Exaggeration Scale of 20
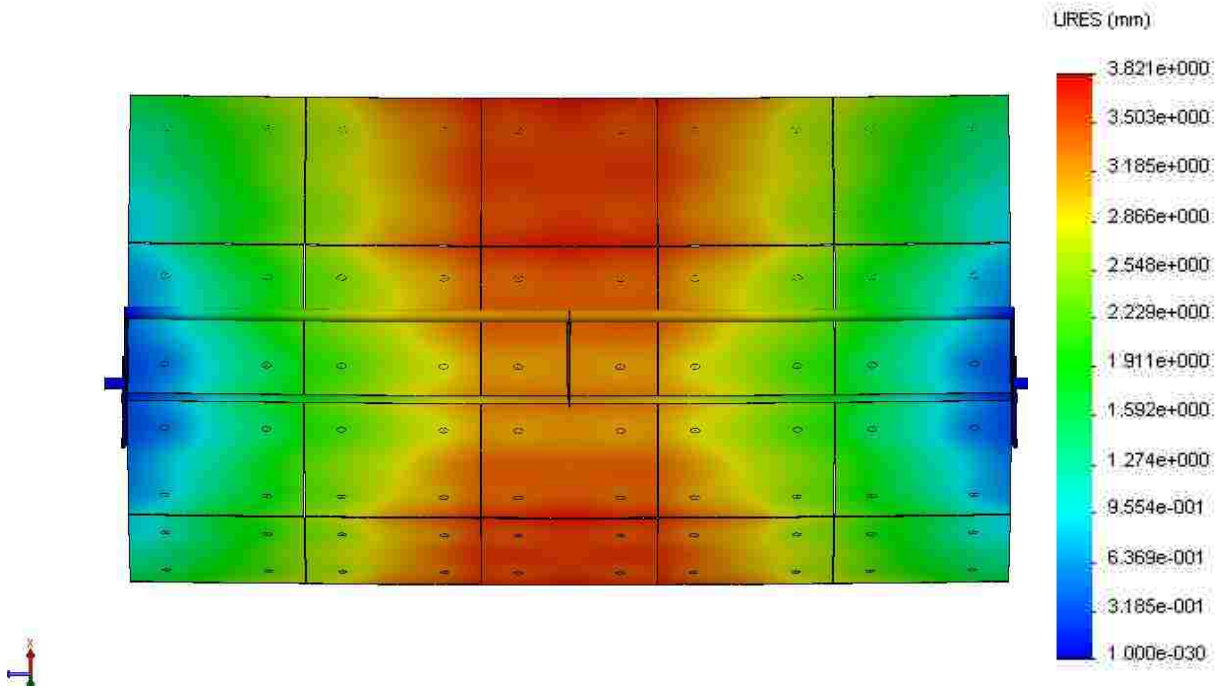
Figure 33: 90° deformed parabolic trough looking at a near top-down angle Exaggeration Scale of 20
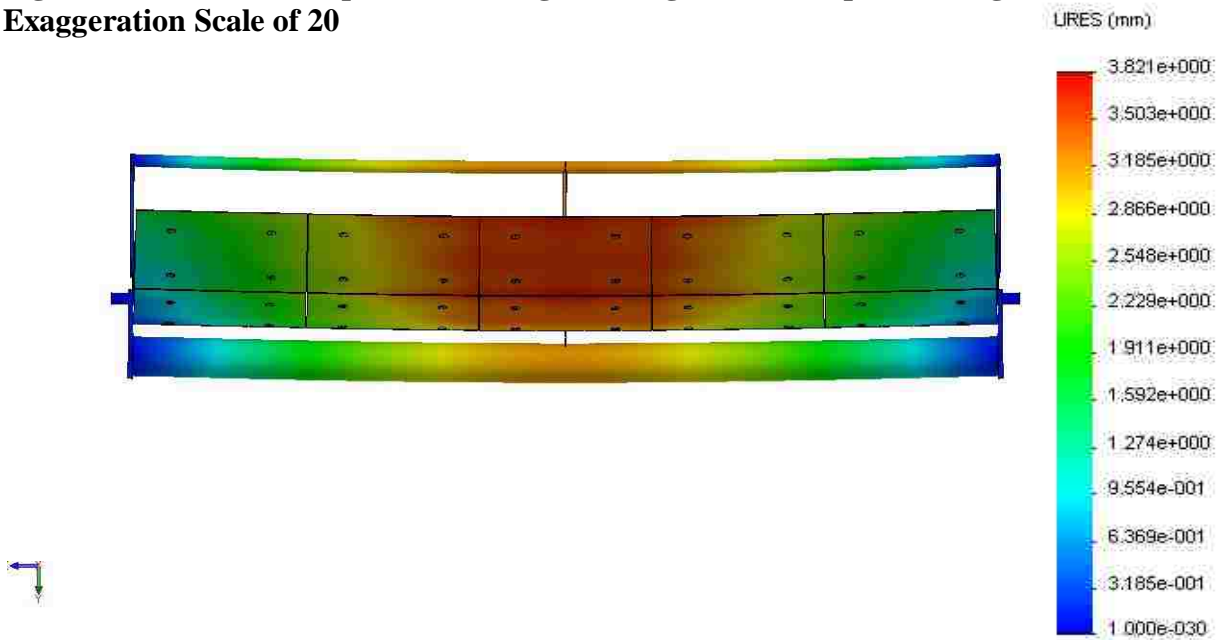
Figure 34: 90° deformed parabolic trough looking perpendicular to the HCE and Torque Tube, Exaggeration Scale of 20
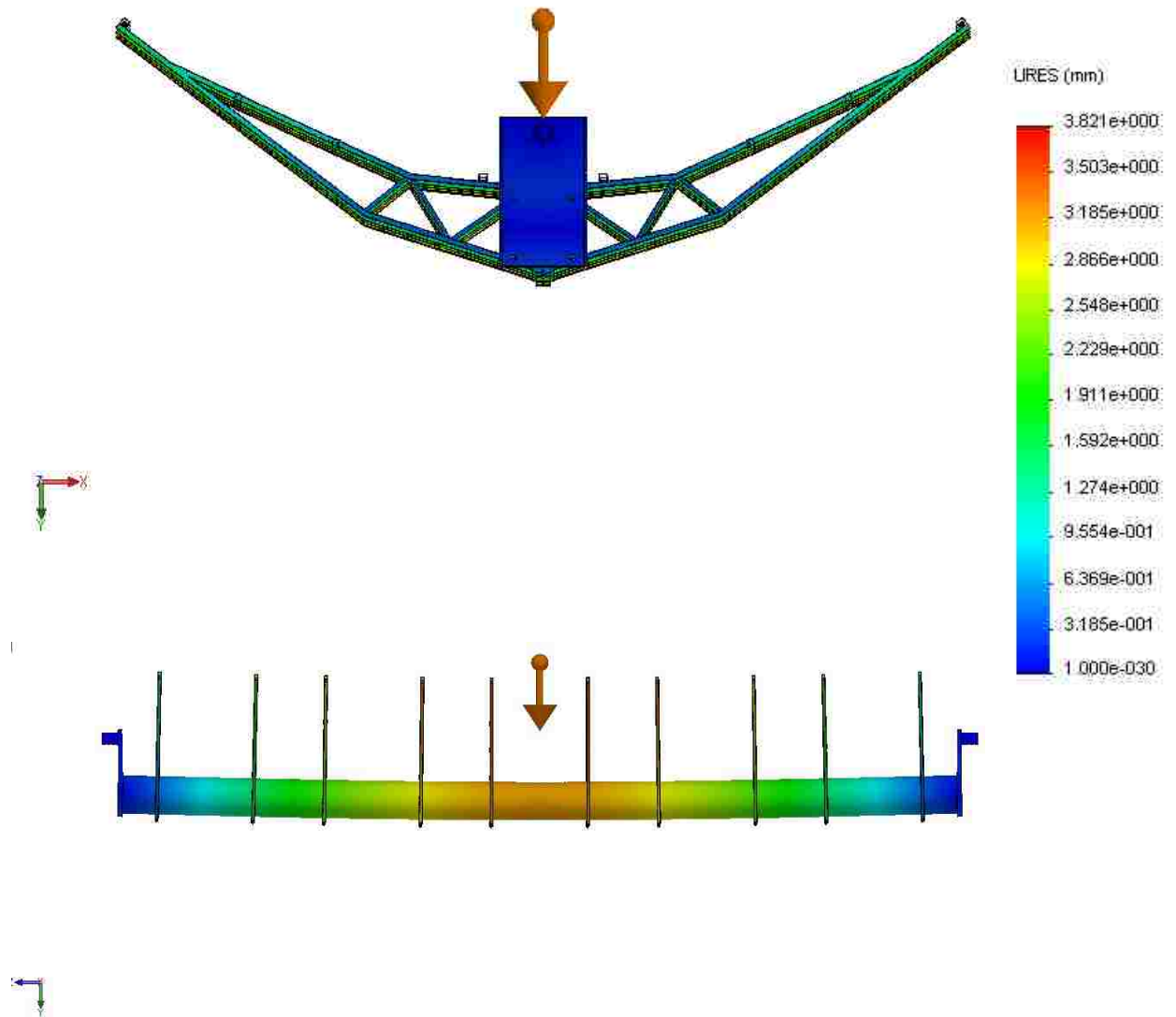
Figure 35. 90° deformed parabolic trough trusses and torque tube displacement plots for full trough module, (Top) View normal to Z-axis, (Bottom) View normal to X-axis, Exaggeration scale of 20, Block arrow indicates gravity load direction

The interesting portion of the FEA analysis are the induced slope errors caused by gravity loading. Six mirrors are evaluated for the surface slope errors. These six mirrors are representative of the entire trough module because of the symmetric nature of the displacements whilst in this position. Figure 36 gives a map detailing the labeling of the mirrors for the slope error analysis.

71

Figure 36: Full parabolic trough labeling map corresponding the mirrors evaluated in the slope error analysis

Table 10 describes the significant statistics of the slope errors on the mirrors. The maximum slope error and the largest average slope errors appear in Mirror 4. Mirror 1 and Mirror 4 are the mirrors on mirror column 1 of the trough indicating that being so close to the ground supports causes these mirrors to have large slope errors. These slope errors are lower than those presented by Ulmer [5] and Wendelin [7] which the nominal slope errors reported are ~3 mrad. However, the simulation slope errors only include gravity deformation which indicate that the nominal slope errors for the trough ranging from 0.5-1.4 mrad are reasonable when compared to actual trough studies. An important factor to remember is that the mirrors have slope errors due to manufacturing, assembly, and cleanliness. Additional slope errors will be applied in the ray tracing analysis to account for these additional factors.

Table 10: Reflective surface slope errors of the full parabolic trough under gravity loading in the 90° position

	Mirror 1	Mirror 2	Mirror 3	Mirror 4	Mirror 5	Mirror 6
Max	6.182	4.740	5.629	7.124	4.985	5.746
Average	1.111	0.746	0.458	1.377	0.997	0.528
Median	0.777	0.546	0.374	0.885	0.761	0.463
St. Dev.	1.057	0.715	0.393	1.259	0.835	0.380

6.2.2   Ray Trace Results

Ray trace modeling was used to predict degradation of the optical performance for the parabolic trough at increasing solar incident angles. The 90° deformed model was used as the basis for the ray trace analysis. Several days were simulated which give characteristic solar incident angles which can be used to compare to the empirical data presented by Dudley [1] for the parabolic trough. As mentioned previously, the glass envelope was excluded from this analysis due to uncertain anti-reflective coating values, but there is empirical data which excludes the glass envelope also.

With increasing incident angles, degradation in optical performance is unavoidable. This is mainly due to cosine foreshortening of the parabolic trough. During the parabolic trough testing, the end losses in the trough are reported to be eliminated from the efficiency experiment. At incident angles other than 0°, there is some portion of the receiver that does not have any incident solar energy. The receiver is thus shortened by this amount when the efficiency calculations were evaluated. The incident angle modifier, which is used to calculate intercept factors, is calculated by dividing the efficiency calculated at any incident angle by the efficiency calculated at a zero incident angle. Thus, end losses are accounted for in the experiment by shortening the length of the HCE in the efficiency calculations. The intercept factors are based on a heat transfer

analysis which proves difficult to compare directly to a ray trace analysis because of thermal losses. The experiment used cold water as the heat transfer fluid and was operated close to the ambient temperature to avoid thermal losses. Also, the focal length and collector reflective area is different in the experiment. The focal length, rim angle, and collector reflective area for the experiment are 1.84 m, 70˚, and 39.2 m^2, respectively. The focal length, rim angle, and collector reflective area for the simulation are 1.49 m, 80˚, and 42.65 m^2, respectively.

The empirical data is adjusted to account for end losses by modifying the efficiency equations of the trough based on a focal length of 1.84 m. However, in the simulations, the focal length is 1.49 m which means the simulations need to be adjusted to more closely match the experimental data. The experimental data is over corrected for when compared to the smaller focal length simulation trough. This geometric difference will cause differences in the intercept factors. The difference in focal length efficiency corrections is shown in Figure 37.
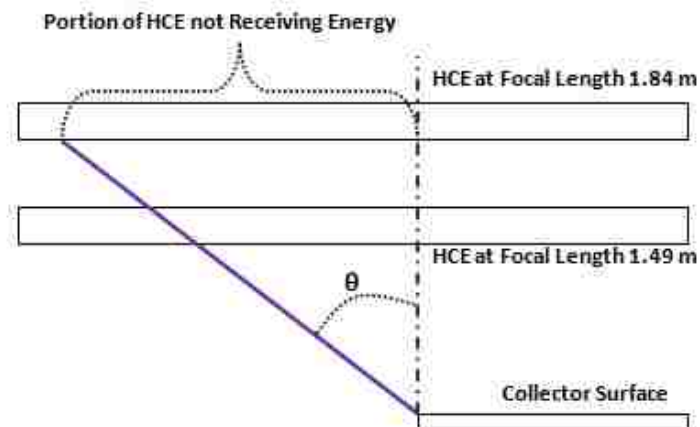
Figure 37. Schematic indicating differences in focal length efficiency calculation corrections between the experimental trough and simulation trough, θ is the incident angle, 1.84 m is the experimental focal length, 1.49 m is the simulation focal length

In the simulations, to account for differences from the experimental setup, the HCE length is adjusted to different lengths to get a representative HCE length corresponding to the experiments. Adjusting the HCE length will essentially calibrate the ray trace simulations for direct comparison to the experimental data. The adjustment accounts for the focal length end loss correction difference between the experiment and simulations. If this is done, the simulation data falls matches closely with the experimental intercept factor data. Four different HCE lengths are evaluated in this study to provide a range of possible HCE lengths.

During the ray trace, several different HCE lengths were chosen to simulate the optical performance seen during the tests. The first length is only the length of the trough. The second length is with a 4 inch HCE extension added to the ends of the parabolic trough length HCE. This is the actual size of the experimental HCE. The third length is with a 30 inch HCE extension added to the ends of the parabolic trough length HCE. Finally, the fourth length is a very long extension added to the ends of the HCE which effectively acts as an infinite length HCE and is a conservative estimate. The infinite length HCE is expected to give better optical results since the end losses are absorbed completely.

As can be seen if Figure 38, there are six ray trace simulations and the empirical data curve for intercept factors for increasing solar incident angle. The infinite length HCE provides very good optical performance with high intercept factors even with solar incident angles up to 58.32°. Even with additional slope errors added to the reflective surfaces, the intercept factors do not match well with the empirical data. The ray trace simulations with an HCE the same length as the parabolic trough have the same trend as

the empirical data. However, the values for the intercept factors are well below the empirical intercept factors, even for the small incident angle of 11.43°. The study with an HCE extended 4 inch past the length of the trough provides similar results as the trough length HCE, but the intercept factors are slightly higher. The 4 inch extended HCE would be the correct ray trace to use if utilizing this data specifically for design purposes. Finally, when running an analysis with an HCE 30 inches longer than the trough collector, the simulation data is close to the empirical data. This trough HCE length calibrates the ray trace simulations to what is being seen in the experiments.

The percent differences between the simulation with a 30 inch extended HCE and experiment range from 0.03% to 2.5% (Table 11). It is noted that the experimental data incident angle modifiers used for empirical intercept factor calculations have an estimated error of +/- 1.88%. An estimation of the additional RMS slope errors actually present on the experimental trough, based on the ray trace simulations, could range from ~2 mrad to ~4 mrad. Any value above 4 mrad would degrade the optical performance too much and any value below 2 mrad is physically unreasonable. It is believed that additional slope errors present on the mirrors for the experimental setup due to reasons other than gravity sag are closer to 2-2.5 mrad based on ray trace results.

Table 11. Intercept factor percent differences between empirical data and trough simulation with 30 inch extended HCE, 2 mrad additional RMS slope errors on mirrors

Incident Angle (°)	Percent difference
11.43	0.77%
35.27	2.54%
48.65	0.03%
58.32	2.28%

Figure 39 and Figure 40 are representative ray traces at two solar incident angles corresponding to days 172 and 355 of a normal year. They are for 2 mrad additional slope error on the 90˚ deformed model with a 30 in extension on the HCE. As can be seen, the HCE extension has little effect for the smaller solar incident angle, but when the incident angle is large the HCE length is important for end loss considerations.
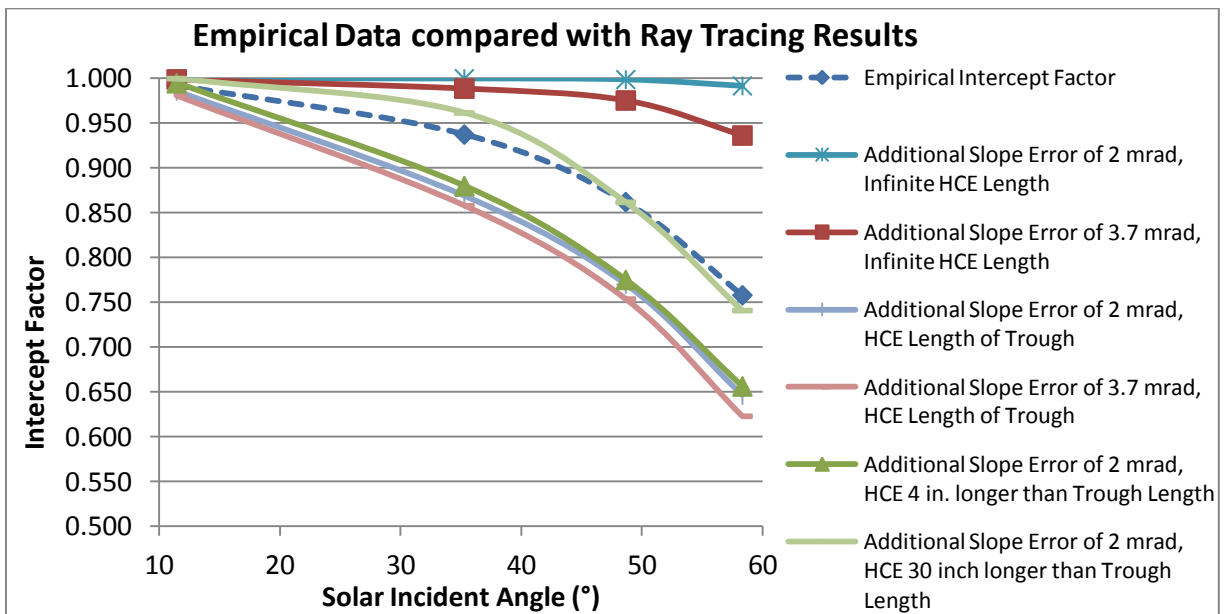
Figure 38: Empirical Intercept Factors compared to Ray Trace Simulation Intercept factors for 90˚ positioned deformed trough
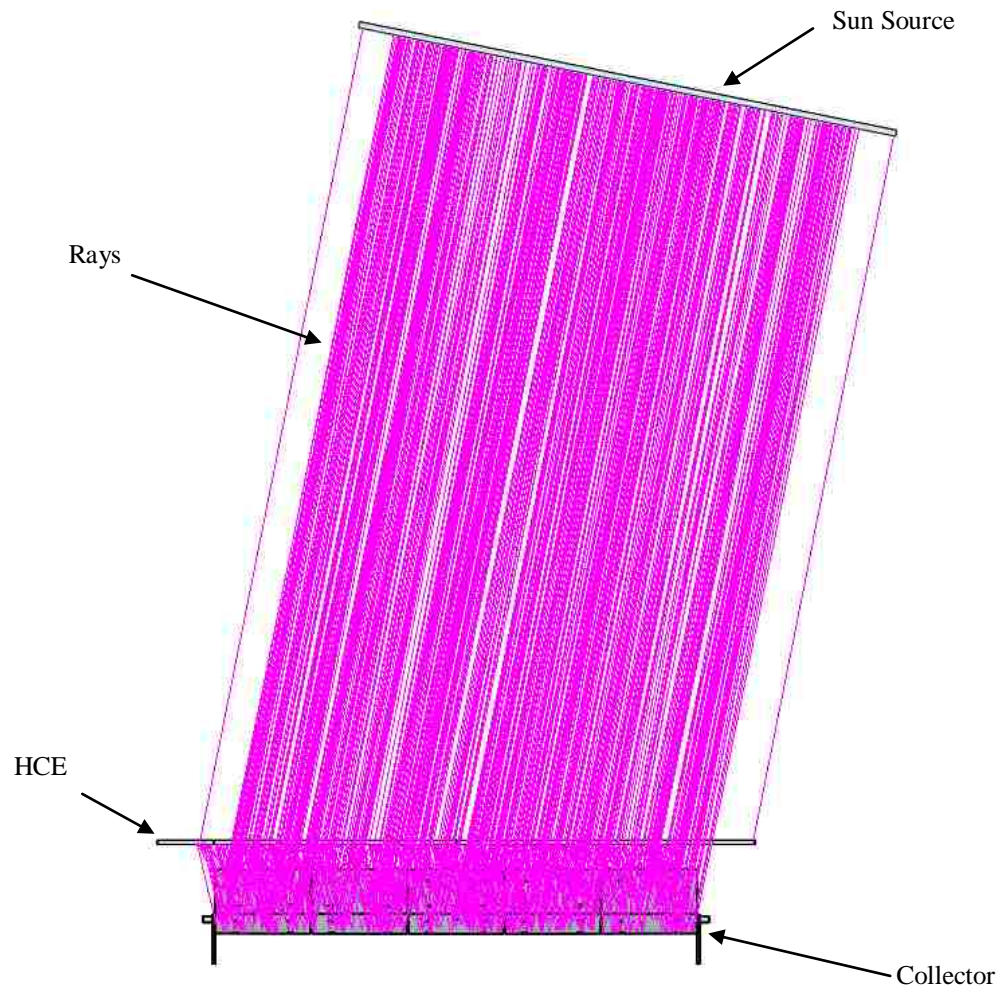
Figure 39: 90 degree deformed model with 2 mrad additional RMS slope errors on the reflective surfaces for 11.43˚ incident angle (Day 172), 30 in. extension on HCE
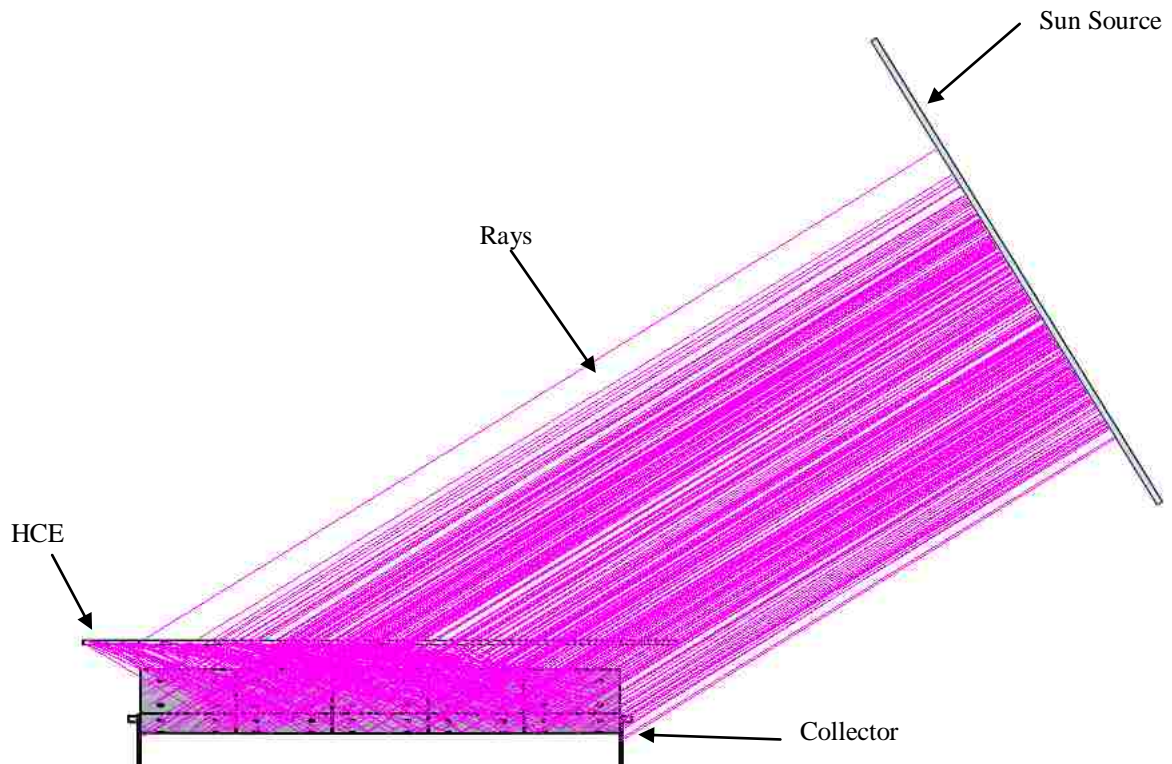
Figure 40: 90 degree deformed model with 2 mrad additional RMS slope errors on the reflective surfaces for 35.27° incident angle (Day 355), 30 in. extension on HCE

6.2.3   Full Trough Module Conclusion

The full LS-2 parabolic trough was run through FEA and ray tracing to estimate the amount of slope error present in the reflective surfaces. The glass envelope was excluded due to data being available for the envelope exclusion during the experiment. Different HCE lengths were evaluated to provide an estimate to which calibrates the simulations to the experimental data well.

The slope errors due to gravity are on average 0.5-1.4 mrad for the mirrors. When including additional RMS slope errors of 2 mrad on the mirrors and an HCE which extends 30 inches beyond the length of the parabolic trough, the intercept factors are

close to experimental data. An estimate of ~2-4 mrad of additional slope errors are present on the experimental trough mirrors based on the ray tracing results for the full trough module. Combining FEA and ray tracing gives a way to predict optical performance of a parabolic trough.

The gravity induced slope errors can be evaluated from a structural standpoint and the trough structure can be adjusted to counter-act the gravity induced errors. The ray tracing can predict the new structure optical performance and thus an iteration process can aid in designing the structure until a final design is acceptable. This process reduces the number of required prototypes and reduces design costs.

7. CONCLUSION

A procedure which couples FEA and ray tracing to predict optical performance of solar collectors has been described and demonstrated. The process can be used for any solar collector and predict optical performance of the collector. This research demonstrated the procedure for a simple single mirror column of an LS-2 trough. The intercept factor results suggest that gravity induced deformations do not affect optical performance when the deformed models were compared to the ideal (undeformed) model. The intercept factors from empirical data for a full trough module were not accurately compared to the single mirror column. This result showed that the single mirror column cannot act as an optical performance indicator for a full trough module. To fully validate the procedure, a full LS-2 trough module was simulated.

The full LS-2 trough module was modeled and compared to the empirical data available. The maximum slope errors present on the reflective surfaces ranged from ~4.7-7.1 mrad while the average slope errors were ~0.4-1.4 mrad. These average slope

errors are less than reported by other studies, [4], [5], [6] and [7], but are thought to be reasonable considering that those studies include slope errors from other sources such as manufacturing defects and assembly procedures. Comparing to the other studies indicates that the additional RMS slope errors on the mirrors could range from ~2-4 mrad.

The deformed models were used as inputs in ray tracing simulations and compared to an ideal (undeformed) model. Additional RMS slope errors were added to the reflective surfaces of the models to evaluate whether gravity induced slope errors contribute to degradation in optical performance with a solar incident angle of 35.27°. The intercept factors showed that gravity induced deformations contribute to degradation in optical performance especially with higher additional RMS slope errors present on the mirrors. The final step in the analysis of the full trough module was comparing the optical results from the simulation directly to the empirical data available. After calibrating the ray trace simulations to match the experimental setup, it was determined that the ray trace simulations are similar to the empirical results. The maximum percent difference in intercept factors was ~2.5% and the minimum percent difference was ~0.03%. The ability for the simulations to resemble empirical data shows that the procedure of coupling FEA and ray tracing provides results that can be used in the collector design process.

In terms of design, the LS-2 trough module has low average slope errors across the reflective surfaces due to gravity loading. It appears that additional RMS slope errors on the mirror surfaces could range from ~2-4 mrad. This result indicates that if the manufactured mirrors have reduced slope errors, then the optical performance of the

trough would increase. The LS-2 could be modified structurally to add additional support to the mirrors to reduce gravity induced slope errors, but this would increase the weight and cost of the trough. The slope errors and displacements discovered by FEA could help alignment procedures for this particular trough which could increase optical performance of the system.

Beam shape, intercept factor, and flux maps can also be generated using the procedure presented in order to predict how a structure behaves under gravity loading. The results can be used to make design changes before prototypes are developed. One particular use of the procedure to aid in design processes was utilized by SkyFuel, which requested that the slope error analysis be performed. This procedure can be useful for designing structures and improvement of optical performance of the system. Using this procedure can result in significant cost savings by adjusting the design before production.

Additional simulation factors could be further studied to improve the procedure presented throughout this research. All of the additional slope errors were uniform across the mirrors of the trough. Each mirror could have more or less additional slope errors present than its neighboring mirrors. This could impact intercept factors. The ray traces could be analyzed further to predict and study some heat transfer values such as absorptivity of the mirrors and HCE. The glass envelope could further be included in the ray trace to study the specific refractive effectives it has on rays reaching the absorbing tube of the HCE for the full trough module. This future work could lead to improvements for this procedure which could further enhance the design process of solar collector systems.

8. RECOMMENDATION OF FUTURE WORK

The future of concentrated solar power technologies is promising. There is a large push for development of these technologies in order to compete directly with fossil fuel electricity production. The current SunShot initiative is to achieve a level zed cost of electricity (LCOE) of $0.06/kWh by 2020 for parabolic trough and power tower technologies [21]. Current trough estimated LCOE in 2015 is for $0.194/kWh and power towers are estimated at $0.144/kWh in 2015 [21]. Many CSP technology goals are outlined in the DOE initiative and can be further studied in the SunShot report by DOE's Energy Efficiency and Renewable Energy department [21].

The current push by DOE has directly influenced the concentrated solar energy research around the country by encouraging scientists and engineers to create new ideas or renovate existing technologies to meet the very ambitious SunShot cost goal. The research presented in this work can be used in any of the concentrated solar collector technologies to evaluate new designs with quick iterations to initially predict optical performance. However, it seems that power tower technologies using heliostats and high temperature receivers are the best option for the CSP industry. New heliostat designs which reduce cost of the collector are starting to emerge. Predicting the optical performance of these designs are critical in power plant design. Initial power tower plants using heliostats are being constructed today with a main one being Ivanpah by Bright Source [22]. Some heliostats are being placed up to 1 mile away from the focal target which has the possibility of reduced optical performance with even the slightest deviation in tracking, structural deformation, or mirror accuracy. The structural analysis is critical to the success of heliostats especially when they are placed at large distances

away from the target. Design iterations can be performed an structural design concepts for these heliostats and predict optical performance of the collector. This would be a next step for this research.

An interesting concept which can also be performed is to parametrically study all of the effects in a collector that affect the optical performance. Design charts/tables can then be created which would be useful in engineering design of future solar collectors. The procedure developed in this research would be a good way to accomplish this task. Many different factors can affect the optical performance of collectors such as mirror roughness, anti-reflective coatings, thermal sagging, etc. These factors can be accounted for in the FEA and ray tracing coupling procedure to analyze all factors affecting optical performance.

An interesting extension to this procedure would be to combine it with high temperature receiver heat transfer analysis using computational fluid dynamics (CFD) software. High temperature receivers can consist of several different receiver types employing different HTFs. The lowest temperature option is utilizing molten salt as the HTF in a recirculation serpentine pattern through HTF tubes exposed to solar flux. A volumetric air receiver can be used to heat air to high temperatures to drive power cycles. A CO_2 HTF can be used in a super-critical gas cycle to drive power cycles. Finally, an interesting option is to use solid particles to absorb solar flux. The solid particles absorb energy to achieve high temperatures and then can be used to drive thermal cycles. All of these receivers can be analyzed in CFD.

The optical performance can be performed to yield accurate irradiance distributions on solar receivers to see how distributed fluxes affect thermal efficiency of receivers.

The optical performance predictions and heat transfer analysis done with receivers can be iterated together in order to get the most efficient solar thermal energy generating system. Higher temperatures will lead to higher thermal efficiency leading to more electricity production. This could lead to improved power plant costs which is critical for achieving the SunShot goal of $0.06/kWh.

REFERENCES

[1] Dudley, V.E., G.J. Kolb, A. R. Mahoney, T. R. Mancini, C.W. Matthews, M. Sloan, D. Kearney. Test Results: SEGS LS-2 Solar Collector. SAND94-1884. Sandia National Laboratories, Albuquerque, NM.

[2] Harrigan, R.W., W.B. Stine. Solar Energy Fundamental and Design. John Wiley and Sons, Inc. 1985.

[3] National Solar Thermal Test Facility Photo and Document Database. <https://energylan.sandia.gov/>

[4] Lüpfert, E., S. Ulmer, K. Pottler, A. Neumann, K.-J. Riffelmann, B. Schiricke. 2007. Parabolic Trough Optical Performance Analysis Techniques. *J Solar Energy Engr.*, 129, 147-152.

[5] Ulmer, S., B. Heinz, K. Pottler, E. Lüpfert. 2009. Slope Error Measurements of Parabolic Troughs Using the Reflected Image of the Absorber Tube. *J. Solar Energy Engr.*, 131, 011014.1-011014.5.

[6] Diver, R.B. and T.A. Moss, 2007. Practical Field Alignment of Parabolic Trough Solar Concentrators, *J. Solar Energy Engr.*, 129, 153-159.

[7] Wendelin, T.J., 2005. Parabolic Trough Optical Characterization at the National Renewable Energy Laboratory, NREL/CP-550-37101, National Renewable Energy Laboratory, Golden, CO.

[8] Jones, S.A. , Gruetzner, J.K., Houser, R.M., Edgar, R.M. and Wendelin, T.J., 1997, "VSHOT Measurement Uncertainty and Experimental Sensitivity Study," Proceedings of the Thirty Second Intersociety Energy Conversion Engineering Conference, Vol. 3, July 27– August 1, pp. 1877-1882.

[9] Lüpfert, E., A. Neumann, K-J. Riffelmann, S. Ulmer. Comparative flux measurement and ray tracing for the characterization of the focal region of solar parabolic trough collectors. Solar Eng. 2004, 689-694.

[10]   He, Y., J. Xiao, Z. Cheng, Y. Tao. A MCRT and FVM coupled simulation method for energy conversion process in parabolic trough solar collector. Renewable Energy, 36 (2011), 976-985.

[11]   Rabl, Ari. Solar Collectors, Energy Storage and Materials (Francis DeWinter, Editor). MIT Press. 1990. "Optical Theory and Modeling of Solar Collectors".

[12]   Mottram, J.T., C.T. Shaw. Using Finite Elements in Mechanical Design. McGraw-Hill Book Company, UK. 1996.

[13]   Moya, A., C. Ho. Modeling and Validation of Heliostat Deformation due to Static Loading. ASME Conf. Proc. ES2011, doi:10.1115/ES2011-54216.

[14]   Dunder, V.D. Structural Analysis of Second-Generation Heliostats. SAND81-8023. 1981. Sandia National Laboratories.

[15]   Welford, W.T., R. Winston. Solar Energy Handbook (J. Kreider and F. Kreith, eds.). McGraw-Hill, New York. 1981. "Principles of Optics Applied to Solar Energy Concentrators".

[16]   Eames, P.C., B. Norton. 1993. Validated, Unified Model for Optics and Heat Transfer in Line-Axis Concentrating Solar Energy Collectors. *Solar Energy*, 50, 339-355.

[17]   Kalogirou, S. A., C.C. Neocleous, C.N. Schizas. 1996. A Comparative Study of Methods for Estimating Intercept Factor of Parabolic Trough Collectors. Conf. Proc. EANN, pp. 5-8.

[18]   Duffie, J., W. Beckman. Solar engineering of thermal processes. John Wiley &

Sons, Inc. Second edition. 1991.

[19]   Pettit, B., C. Ashley, S. Reed, C. J. Brinker. "Antireflective films from the Sol-Gel

Process." Sol-Gel technology for thin films, fibers, performs, electronics and

specialty shapes. Ed. Lisa Klein. Noyes Publications. 1988.

[20]   SkyFuel Inc. 2012. 12 Feb. 2012 <http://skyfuel.com/#/HOME/>.

[21]   Department of Energy. Energy Efficiency and Renewable Energy. Feb. 2012. 4

Apr. 2012 <http://www1.eere.energy.gov/solar/pdfs/47927_chapter5.pdf>

[22]   Bright Source. 2012. 11 Apr. 2012.

<http://www.brightsourceenergy.com/projects/ivanpah>